2010

Ferromagnetism and transport in diluted magnetic semiconductors

Abdolmadjid Nili
Louisiana State University and Agricultural and Mechanical College

FERROMAGNETISM AND TRANSPORT IN DILUTED MAGNETIC SEMICONDUCTORS

A Dissertation

Submitted to the Graduate Faculty of the
Louisiana State University and
Agricultural and Mechanical College
in partial fulfillment of the
requirements for the degree of
Doctor of Philosophy

in

The Department of Physics and Astronomy

by
Abdolmadjid Nili
B.S., Sharif University of Technology, 1999
M.S., University of Cincinnati, 2006
August 2010

Acknowledgments

This research project would not have been possible without the support of many people. The author wishes to express his gratitude to his advisor, Prof. Mark Jarrell who was abundantly helpful and offered valuable assistance, support and guidance. Deepest gratitude are also due to Prof. Juana Moreno without whose knowledge and guidance this study would not have been successful. Special thanks to Prof. Dana Browne for his insightful ideas and endless support. Finally, the author would like to convey thanks to his colleagues Mohammad Majidi, Peter Reis, Shuxiang Yang, Unjong Yu, Zhaoxin Xu, and Dimitris Galanakis.

Table of Contents

Abstract

This dissertation focuses on the study of ferromagnetism in Dilute Magnetic Semiconductors. To study these strongly correlated electronic systems, two non- perturbative techniques are used: the Dynamical Mean Field Approximation (DMFA) and the Dynamical Cluster Approximation (DCA). The model used for Dilute Magnetic Semiconductors (DMS) incorporates the strong spin-orbit couplings of the carrier holes as found in most III-V semiconductors doped with manganese such as $Ga_{1-x}Mn_xAs$. Calculated within the DMFA, the spin-orbit coupling effects give rise to various interesting physics, primarily the anisotropic behavior of the impurity band that affect the charge transport properties in the ferromagnetic phase. We show that non-local correlations, within the DCA, are responsible for magnetic frustration and magnetic reorientation of the DMS. The DMFA is employed to study ferromagnetism and transport in $Ga_{1-x}Mn_xAs$, using the sp^3 tight-binding Hamiltonian. Finally, employing the sp^3 tight-binding Hamiltonian and the DMFA, ferromagnetism in a wide band gap $Ga_{1-x}Mn_xN$ is studied.

Chapter 1

Introduction

1.1 New Magnetic Material For Spintronics

The motivation for this study has been to better understand the material which could be the building block for the next generation of computers. According to Moore's law the number of transistors in a chip doubles every eighteen to twenty two months. At this rate, very soon, the size of a transistor will not exceed several atoms. Thus, our ability to make faster processors is limited by the transistor size. In order to overcome the shortcoming of conventional electronics the idea of spintronics was proposed. Spintronics utilizes both charge and spin of the electrons to process and store data. Spintronics based transistors have several major advantages over todays transistors, among them are their ability to integrate data process and storage in a single step and controlling of spin currents with an external magnetic field. In fact, the idea of using electron spin has already revolutionized data storage device technology as we use giant magneto-resistant devices everyday such as hard-disks and RAM memories. One should keep in mind that these memory devices are based on static spin as opposed to data processing units which are based on spin currents.

Recently, ferromagnetic semiconductors have become a major focus in both academia and industry as these materials might form the base of spintronics. As conventional electronics, semiconductors are more appropriate than normal metals, since metal devices do not amplify current. Moreover, mixed devices (based on metal and semiconductors) have problems with spin injection due to the large scattering cause by the conductivity mismatch at the interface between the ferromagnetic metal and semiconductor. Magnetic semiconductors that act as spin-injectors might be the solution for the above problems.

In magnetic semiconductors a conventional semiconductor e.g. GaAs or GaN is doped heavily (doping $\sim$5%-10%) with magnetic ions such as manganese (Mn). Upon doping each magnetic ion preferably substitutes a cation and introduces a local magnetic moment, as well as an extra hole due to the mismatch of the electronic structure of the two ions. These holes are loosely bound to the acceptor ions, thus propagate throughout the system. They interact with the magnetic ions, d orbitals, via the $p-d$ hybridization.

Since the magnetic impurity concentration is small in the diluted magnetic semiconductors (DMS), magnetic interactions in the material are mostly mediated by itinerant holes, which aline magnetic moments ferromagnetically.

In the DMS, magnetic impurities are randomly scattered, thus make the material highly disordered. Furthermore, the magnetic exchange interaction is strong and comparable to the Fermi energy. As the result, the DMS fall under category of strongly correlated systems where static mean-field approach is too simplistic to capture the complexity of the material.

1.2 Background

1.2.1 Strongly Correlated Electronic Systems

In general strongly correlated electronic systems are many-particle systems in which the short interaction (U) between constituent electrons is a major factor in defining the behavior of the material. If we define W as the bandwidth of the dispersion band which appears from the hybridization of the atomic orbitals at different sites, in strongly correlated systems the ratio U/W becomes large. In such systems the single particle approach fails, and one has to take into account the collective behavior of particles since the motion a one particle is greatly affected by the interaction with other particles in the system. This fact increases the level of complexity of the system to the extent that there are no analytical solutions for strongly correlated systems except for very limited and specific cases. Examples of strongly correlated systems include, but are not limited to, cuprates, rare-earth systems, diluted magnetic semiconductors and transition-metal oxides.

An interesting example to showing the importance of correlations between the electrons is the Mott insulator. Mott insulators are conductors according to band structure calculations (where the correlations between the electrons are limited to the Pauli exclusion principle). But experiments show that such systems are in fact insulators, particularly at low temperatures. This phenomenon has been observed in transition metal oxides that have partially filled d orbitals. Mott proposed [8] that the strong local repulsion between the d electrons prevents the hopping of electrons from one site to the other, thus, the material does not conduct electricity.

Various models have been proposed for strongly correlated systems such as the Hubbard model where the electron-electron interaction is treated as a simple onsite interaction (U) and the overlap of the adjacent atomic orbitals is taken into account by hopping integrals which in general depend on the orbital type. Despite its simplicity even the single band Hubbard model (with just one orbital per site) does not have an

analytical solution except in one and infinite dimensions. Other interesting strongly correlated systems are metals with magnetic impurities, i.e transition metal or rare earth ions with partially filled d (or f) orbitals. The localized d (or f) orbitals hybridize with the conducting s or p orbitals of the adjacent sites. This is in addition to the strong onsite repulsion among local d (f) electrons. The Kondo [9] and Anderson [10] models are proposed to describe anomalies in the transport and magnetic properties of such systems. For example, for many years physicists were puzzled by the anomaly in the low temperature resistance of systems with magnetic impurities in non-magnetic metals, where resistivity rises under specific low temperature T_K (Kondo temperature). This effects could not be explained by models based on single particle scenarios. It was Kondo who suggested that the anomaly is due to correlations amongst electrons in the system. He explained it by considering the spin-flip scattering off the electrons from magnetic impurities. By introducing the spin degree of freedom for the electrons, the Kondo model essentially brings back the Pauli exclusion principle (a many-body effect) to the electron scattering from a magnetic impurity. According to the model, at low temperature, the screening of the magnetic impurities by electrons is less effective thus the resistivity increases.

The focus of this dissertation is on the diluted magnetic semiconductors. The double-exchange interaction, which shares general ideas with the Kondo model, is adopted to model the magnetic interactions in the DMS. The DMS are strongly correlated systems in because the $p-d$ exchange coupling is larger than the Fermi energy. The complexity of the system is increased by the random distribution of magnetic impurities throughout the system.

1.2.2 Diluted Magnetic Semiconductors

Ferromagnetic semiconductors have been in the center of much attention for more than a decade[11, 12, 13] due to their interesting physical properties and potential device application in spintronics [14, 15]. The main idea is to combine semiconductor physics and magnetism, which have been among the well established areas of condensed matter physics. The newly developed field of spintronics utilizes both the charge and the spin degree of freedom of the charge carriers (electrons or holes) to integrate processing and storage of data. However, in order to control the magnetic and transport behavior of the magnetic semiconductor one has to address many parameters such as the $p-d$ exchange interaction (J_{p-d}) between the $d-$level electrons (holes) of the impurity and the $p-$type valence electrons (holes). The problem is that semiconductors are extremely sensitive to impurities and any other external (e.g. fields) or internal (e.g. defects) parameter. Thus growth of magnetic semiconductors should be under considerable control. Another issue is these materials are

highly disordered since a high ferromagnetic transition temperature is reached once they are heavily doped ($\sim 5\% - 10\%$). This makes the study of the DMS more challenging. Moreover, the issue of solubility of the magnetic ions into the regular semiconductor was a major challenge to fabricate high quality diluted magnetic semiconductors. Fortunately, in recent years, advances in non-equilibrium techniques such as Molecular Beam Epitaxy (MBE), have led to the successful growth of various DMS including (Ga,Mn)As and (Ga,Mn)N with Curie temperatures as high as 250K in nanostructures and 370K in heterostructure DMS [16, 17, 18, 19]. This thesis focuses on the group III-Mn-V ferromagnetic semiconductors, more specifically $Ga_{1-x}Mn_xAs$ and $Ga_{1-x}Mn_xN$. It has been established that several (III,V) compounds can reach ferromagnetic transition temperatures above 100K once they are heavily doped with magnetic atoms.

Since DMS are grown using out of equilibrium techniques a noticeable fraction of magnetic atoms lies not on the preferred site (cation) but on the anion (anti-site) or somewhere in the middle of the crystal (interstitial). While the effect of anti-site ions is to reduce the effective doping and carrier density, the question about the real effect of interstitial ions is yet to be answered. A high percentage of interstitial manganese (Mn_I) in the DMS ($\sim 20\%$ in the highly-doped as grown samples) might lead to significant effects on the properties of the material. It is not clear whether the d orbitals of an interstitial Mn_I hybridize with valence band orbitals of neighboring atoms. There are studies for and against either scenario[20, 21, 22]. Furthermore, it is possible that an interstitial magnetic ion engages in short range antiferromagnetic interaction with neighboring substitutional ion (Mn_{Ga}) to form magnetic dipoles[20, 21]. The direct effect of the magnetic dipoles is the reduction of the effective magnetic moment in the DMS. This is because in dipoles, the short-range antiferromagnetic interaction between ions suppresses the total magnetic moment. Mn_I is also a double donor i.e. each interstitial manganese compensates two holes introduced by substitutional Mn, thus it reduces the effective charge carrier density. In addition to that, interstitial defects can lead to structural changes in the crystal which in turn may affect its ferromagnetic behavior[22, 23]. The percentage of doping defects (anti-site and interstitial) can be brought down by using postgrowth annealing at temperatures close to growth temperature[24, 25, 26, 2].

Early experiments showed that there is an intimate relationship between the ferromagnetic transition temperature and the hole carrier density and hole localization[27, 11, 13]. This led to proposed models that explain the magnetic interaction amongst impurity magnetic moments through mediation by itinerant charge carriers. It is generally accepted that the ferromagnetism in the DMS arises from the Zener double-exchange process[20, 28, 29]. Zener proposed a double-exchange mechanism[30] in order to explain ferromagnetism in a certain class of materials. According to this model the interaction between two isolated magnetic atoms is via

hybridization of their magnetic shell with the orbitals of an intermediate non-magnetic atom. In the case of group (III,Mn)V DMS, Mn represents by its mixed *spd* orbital which hybridize with *sp* orbitals of the parent semiconductor (III-V). In the regimes of small values for kinetic-exchange interaction, ferromagnetism follows the Ruderman-Kittle-Kasuya-Yosida (RKKY) picture [31, 32]. However, there is no significant difference between the RKKY and the double-exchange models. In fact the former is the weak coupling regime of the latter.

Zaránd and Jankó [33] proposed a simplified double-exchange model to study the magnetic behavior of the DMS, represented by the following Hamiltonian:

$$H = H_0 + J_c \sum_i \mathbf{S}(R_i) \cdot \mathbf{J}(R_i) \tag{1.1}$$

For the non-interacting Hamiltonian (H_0) they adopted the $k \cdot p$ Hamiltonian proposed by Luttinger and Kohn [34] where spin-orbit interaction is taken into account by simplifying the Luttinger-Kohn model. The magnetic interaction between the itinerant holes and the local moments in this model is simplified to just a local interaction at the impurity location where the spin of the magnetic ion is treated as classical due to its rather large magnitude (S=5/2). They showed that the bulk DMS is a frustrated ferromagnet.

Although the nature of the magnetic interaction within DMS is still a matter of controversy as noted above, some consensus has emerged regarding the effects of magnetic dopants on the band structure of the parent material specially for the case of $Ga_{1-x}Mn_xAs$[20]. In this material the substitution of cation (Ga^{3+}) with a magnetic ion (Mn^{2+}) introduces an itinerant hole to the system as well as a local magnetic moment ($S = 5/2$) due to its half filled d orbital. Moreover, since the Mn^{2+} ion is negatively charged with respect to the Ga^{3+} ionic background there is an effective attraction interaction between the Mn ion and the charge carriers. In the case of $Ga_{1-x}Mn_xAs$ the filled d orbitals lie deep in the valence band, thus the number of particles in this orbital is fixed. Due to the rather large moment ($S = 5/2$) of the deep valence d orbitals, one can safely assume that the magnetic interaction in the material is between holes and classical-like local moments at each Mn site. The free propagation of the itinerant holes in the DMS is disrupted by the disorder due to random distribution of the magnetic impurities. This leads to the formation of the localized states at the impurity sites. The overlap of these localized states results in the impurity band. The aforementioned magnetic interaction in the DMS, $p-d$ exchange coupling, is mostly mediated by the p-type holes and it is evident that the localized states are made of such carriers. Since in GaN and GaAs the valence band has p-type character, while the conduction band is $s-$like, we expect that the impurity band is formed close to the valence band.

On the other hand in wide band gap semiconductors, such as $Ga_{1-x}Mn_xN$, the role of the magnetic ion is not agreed upon. In this DMS the Mn_{Ga} ions can have two ionizations namely Mn^{3+} ($4d$) and Mn^{2+} ($5d$) with $S = 2$ and $5/2$ respectively. In the former (Mn^{3+}) the d orbital of the Mn lies deep in the band gap and form quasi-local states[35, 36, 37, 38]. The nature of this orbital and whether it hybridizes with $p-$like valence holes is not clear yet. Some studies suggest that these orbitals do not hybridize, and thus do not have a noticeable effect in mediation of magnetic interaction, while others claim the role of the deep valence band d orbitals can not be overlooked[37, 38, 20]. There are also other features that contribute to the complexity of the DMS including formation of magnetic clusters which have a noticeable effect on the magnetic properties of the material, e.g. the reported T_c of $Ga_{1-x}Mn_xN$ is in the range of 2k-900K[39, 19, 38].

This dissertation uses the Zaránd and Jankó Hamiltonian for the magnetic interaction in the DMS. Different Hamiltonians are employed for the parent material in order to establish a more realistic picture of the DMS. We systematically study $Ga_{1-x}Mn_xAs$ and $Ga_{1-x}Mn_xN$ within the framework of the self consistent Dynamical Mean Field Approximation (DMFA). In order to capture effects such as frustration, which originate in the non-local interactions and are ignored in DMFA, we employ the Dynamical Cluster Approximation (DCA). Since the DMFA and the DCA are non-perturbative, they can be used for different regimes of interaction strength. Moreover, both approximations fully take into account the temporal fluctuations at the impurity sites which are crucial, especially in the vicinity of the ferromagnetic transition temperature. These important fluctuations are averaged over in static mean field approximations.

1.2.3 The Dynamical Mean Field Approximation (DMFA)

The DMFA[40, 41] is a self-consistent mean field theory which fully incorporates dynamical correlations among the electrons but ignores all non-local correlations. By ignoring spatial correlation amongst the electrons, the DMFA relaxes the momentum conservation at the internal vertices of the Feynman diagrams. For example in a two-body interaction diagram, the Laue function Δ function is set to 1:

$$\Delta(k_1, k_2, k_3, k_4) = \sum_r e^{ir.(k_1+k_2+k_3+k_4)} = N\delta_{k_1+k_2,k_3+k_4} \to 1 \tag{1.2}$$

It follows that the self energy does not have momentum dependency within the DMFA[42]:

$$\Sigma_{DMFA}(k, \omega) = \Sigma(\omega) \tag{1.3}$$

where ω is the frequency (energy). It has been shown[43] that the DMFA is exact in the limit of infinite

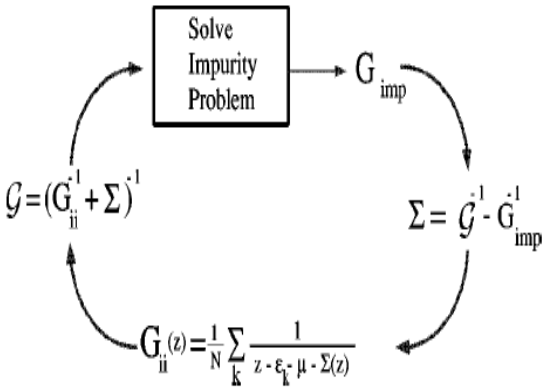

Figure 1.1: The DMFA algorithm

dimensions ($D \to \infty$). One may assume it is a reliable approximation when the number of neighboring sites are large e.g. in the zinc-blende structure where the underlying crystal structure is face centered cubic (FCC) with D=12. However, one has to keep in mind that in systems such as diluted magnetic semiconductors, non-local correlations lead to effects such as frustration, which can have a noticeable effect on the magnetic behavior of the material. So the method carries significant limitations despite the relatively large number of neighboring sites.

Figure 1.1 illustrates the self consistency algorithm for the DMFA as followins:

1. Start by making a guess for the self-energy $\Sigma(\omega)$.

2. Calculate the local Green's function $G_{loc}^{-1}(\omega) = 1/N \sum_k [G_0^{-1}(\omega) - \Sigma(\omega)]$, where G_0 is the non-interacting lattice Green's function.

3. Find the cluster excluded Green's function, $\mathcal{G}(\omega)$, via $\mathcal{G}^{-1}(\omega) = G_{loc}^{-1}(\omega) + \Sigma(\omega)$; this is to avoid the interactions of a particle with itself.

4. The cluster solver calculates the impurity Green's function ($G_{imp}(\omega)$) by using an appropriate technique, here the Coherent Potential Approximation (CPA).

5. Having obtained the impurity Green's function and cluster excluded Green's function, calculate the new self-energy via $\Sigma(\omega) = \mathcal{G}^{-1}(\omega) - G_{imp}^{-1}(\omega)$. Start step 1 with new calculated self-energy and continue the loop until reaching the desired convergency.

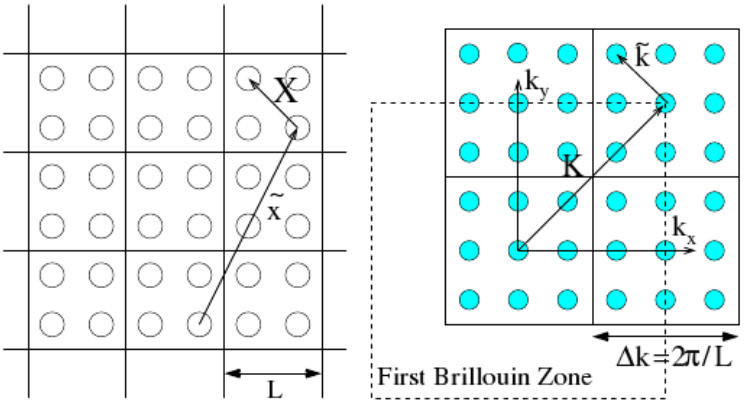

Figure 1.2: Division of real lattice and the first Brillouin zone in DCA ($N_c = 4$)

1.2.4 The Dynamical Cluster Approximation (DCA)

The above-mentioned DMFA ignores all spatial correlations in the system. While those correlations are of less importance in some cases, in many interesting physical systems they have noticeable effects on the material properties. The DCA is introduced [44] to incorporate some of the non-local interactions, relinquished within the DMFA. It systematically restores the momentum conservation at internal vertices, which makes it the natural extension to the DMFA. Within the DCA the Brillouin zone is divided into N_c equal cells where each momenta in the cell is labeled by k= $\mathbf{K}+\tilde{k}$. Here $\mathbf{K}$ is the momenta at the center of the cell and $\tilde{k}$ is the momenta within the cell measured from the cell center.

Figure 1.2 illustrates the tiling for $N_c = 4$. It is clear that the DCA restores the DMFA results in the limit of $N_c \to 1$. Since the DCA does not neglect momentum conservations all together, the self-energy is not completely local:

$$\Sigma_{DCA}(k,\omega) = \Sigma(\mathbf{M}(\mathbf{k}),\omega) = \Sigma(\mathbf{K},\omega) \tag{1.4}$$

where $\mathbf{M(k)}$ maps each momentum (k) to its corresponding cell momentum ($\mathbf{K}$). In the language of Laue function, the partial momentum conservation reads:

$$\Delta(k_1,k_2,k_3,k_4) = N_c\delta_{\mathbf{K_1}+\mathbf{K_2},\mathbf{K_3}+\mathbf{K_4}} \tag{1.5}$$

Figure 1.3 outlines the scheme for the DCA self consistency algorithm. One can see that for the most part the two algorithms (DCA and DMFA) are similar except that the DMFA maps the original lattice to a single site while the DCA maps it into a N_c site cluster. Like the DMFA algorithm we start with some

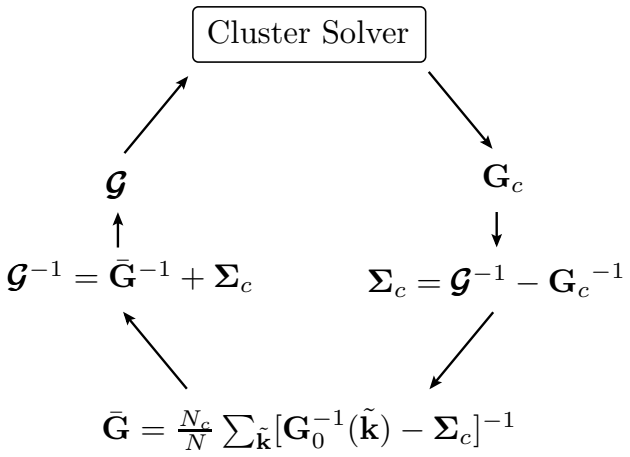

Figure 1.3: The DCA algorithm

guess for the self-energy function (usually zero) and calculate the coarse grained Green's function

$$\bar{G}(\mathbf{K}, \omega) = \frac{N_c}{N} \sum_{\tilde{k}} \frac{1}{\omega - \epsilon_{\mathbf{K}+\tilde{k}} + \mu - \Sigma^c(\mathbf{K}, \omega)} \tag{1.6}$$

where $\epsilon_{\mathbf{K}+\tilde{k}}$ is the dispersion of the non-interacting Hamiltonian and μ is the chemical potential. The cluster excluded Green's function is calculated similar to the DMFA

$$\mathcal{G}^{-1}(\mathbf{K}, \omega) = \bar{G}^{-1}(\mathbf{K}, \omega) + \Sigma^c(\mathbf{K}, \omega) \tag{1.7}$$

The cluster excluded Green's function is the input to the cluster solver, e.g. the CPA, with output of the cluster Green's function ($G^c(\mathbf{K}, \omega)$). The last step is to find the new cluster self-energy.

$$\Sigma^c(\mathbf{K}, \omega) = \mathcal{G}^{-1}(\mathbf{K}, \omega) - {G^c}^{-1}(\omega) \tag{1.8}$$

The self-energy is used to recalculate the coarse grained Green's function and iterations will continue until convergency is reached.

One should be careful in choosing a cluster that satisfies the point group symmetry of the original lattice. Finally, notice that the DCA ignores the dependency of the self-energy on small momenta ($\Sigma^c(\mathbf{K} + \tilde{k}, \omega) = \Sigma^c(\mathbf{K}, \omega)$), so it is a good approximation in the absence of strong short range interactions.

1.3 Outline of Dissertation

This dissertation is organized as follows:

In Chapter 2, the DMFA is employed to study a simplified model for $Ga_{1-x}Mn_xAs$. We use the two-band (heavy and light bands) tight binding Hamiltonian with a cosine dispersion to model the band structure of the parent material. The effect of the attractive Coulomb interaction between the acceptor magnetic impurities and itinerant holes is also studied. It is shown that in general both the Coulomb potential and the magnetic coupling between the magnetic ions and charge carriers enhance ferromagnetism in the DMS. Moreover, a toy model is used to study the effect of strong spin-orbit interaction of the parent compound on the magnetic properties of the material. We conclude that the effect of the spin-orbit interaction on the ferromagnetism is different in weak and strong regimes of the interaction parameters (Coulomb and magnetic coupling). For a small Coulomb potential and magnetic coupling, the spin-orbit interaction enhances ferromagnetism, but it suppresses the ferromagnetic transition temperature at large values of these parameters.

In Chapter 3 we introduce non-local interactions in $Ga_{1-x}Mn_xAs$ by using the DCA technique for several clusters. While mean-field studies capture the main features of the DMS, non-local effects may be equally important for the itinerant carriers, which mediate the effective magnetic interaction in the DMS. It is shown that non-local correlations amongst neighboring magnetic ions lead to magnetic frustration in the DMS. We find considerably lower T_c for the frustrated ferromagnet which is in better agreement with experiment than the DMFA results. Within this model the maximum T_c is reached when the hole concentration is half of the magnetic doping. The DCA also enables us to study the effect of anisotropy on ferromagnetism of the DMS. We investigate the magnetic anisotropy of $Ga_{1-x}Mn_xAs$. We show that while the magnetic anisotropy depends on strain, hole concentration, and temperature in a complicated manner, generally it has in-plane anisotropy with compressive strain and perpendicular-to-plane anisotropy with tensile strain.

In Chapter 4 a more realistic sp^3 tight-binding Hamiltonian for the parent compound is used to study $Ga_{1-x}Mn_xAs$ within the DMFA. Inclusion of the conduction band in the narrow gap GaAs leads to band repulsion, which was absent in our previous DMFA studies. We find that this effect considerably narrows down the impurity bandwidth. As a consequence of narrower bandwidth, holes are more localized thus less able to mediate the magnetic interaction between the magnetic ions. We find more realistic ferromagnetic behavior by employing a more realistic tight-binding Hamiltonian. We also investigate the dependence of the hole polarization on the magnetic coupling strength of the DMS. Moreover, we study the optical conductivity of the DMS for a wide range of magnetic couplings.

In Chapter 5 we employ the DMFA to study $Ga_{1-x}Mn_xN$, one of the most important members of the

wide band gap DMS. GaN has wurtzite crystal structure with two gallium and two nitride atoms in the unit cell. We use the sp^3 tight-binding Hamiltonian for the parent compound. We expect that the effect of band repulsion on the impurity bandwidth is less profound in the wide band gap DMS. We study the ferromagnetism $Ga_{1-x}Mn_xN$ in different coupling regimes. The spin-orbit interaction in much smaller in $Ga_{1-x}Mn_xN$ than in $Ga_{1-x}Mn_xAs$. We investigate the effect of the small spin-orbit interaction on the magnetic frustration through the hole polarization. Furthermore, we study the effect of crystal anisotropy on the ferromagnetic transition temperature of the DMS in the wurtzite structure. We compare our findings for the ferromagnetic transition temperature with the results of the previous static mean-field study.

Finally, Chapter 6, summarizes the achievements in each chapter and outlines possible developments in the future.

Chapter 2

The Effect of Spin-Orbit Interaction and Attractive Coulomb Potential on the Magnetic Properties of $Ga_{1-x}Mn_xAs$

2.1 Introduction

Although the notion of using magnetic semiconductors in spintronic devices dates back to the 1960's [45], the discovery of high temperature ferromagnetism in dilute magnetic semiconductors (DMS)[27, 46] initiated an active search for the optimal compound with a magnetic transition above room temperature. Since these materials are good sources of polarized charge carriers, they may form the basis of future spintronic devices,[14, 15] which utilize the spin of the carriers as well as their charge to simultaneously store and process data. Perhaps one of the most promising DMS is GaAs doped with Manganese due to its rather high ferromagnetic transition temperature ($T_c > 150$ K for bulk samples and ~ 250 K for δ-doped heterostructures[18, 17]) and its wide use in today's electronic devices.

In $Ga_{1-x}Mn_xAs$, the Mn^{+2} ion primarily replace Ga^{+3} playing the role of acceptor by introducing an itinerant hole to the p-like valence band. The strong spin-orbit interaction in the valence band couples the angular momentum to the spin of the itinerant hole resulting in total spin $J{=}l+s{=}3/2$ for the two upper valence bands and $J{=}l-s{=}1/2$ for the split-off band. Each manganese also introduces a localized spin ($S{=}5/2$) due to its half-filled d orbital. In addition, since the Mn^{+2} ion is negatively charge with respect to the Ga^{+3} ionic background there is an effective attractive interaction between the Mn ion and the charge carriers.

In previous studies[47, 48] some of us have explored the effect of the strong spin-orbit coupling on the ferromagnetic transition temperature T_c, the carrier polarization as well as the density of states and spectral functions using the Dynamical Mean-Field Approximation (DMFA). In these studies we used the $k\cdot p$ Hamiltonian to model the dispersion of the parent material (GaAs). While $k\cdot p$ is a good approximation around the center of the Brillouin zone (Γ point), it is a poor one away from it. In this work we improve our model by incorporating a more realistic tight binding dispersion for the valence bands as well as an attractive on-site potential between the Mn ions and the itinerant holes. Moreover, we study the effect of the spin-orbit

interaction of the holes on the magnetic behavior of the DMS. We find that for intermediate values of the exchange coupling both the on-site potential and the spin-orbit enhances the critical temperature, while in the strong coupling regime the spin-orbit interaction significantly suppresses T_c[49].

The effect of the attractive Coulomb potential has been discussed for models with only one valence band, which ignore the spin-orbit interaction,[50, 51, 52, 53] and multi-band tight-binding models, which include spin-orbit coupling, but with a limited sampling of disorder configurations.[54] Here we include on an equal footing the effect of the attractive Coulomb potential using a simple Hartree term, the exchange between magnetic ions and itinerant holes, the spin-orbit coupling, and the disorder within the coherent potential approximation (CPA).[55, 56, 57] We investigate the ferromagnetic transition temperature, the average magnetization of the Mn ions, the polarization of the holes, and the quasiparticle density of states as function of the Coulomb and exchange couplings. First, we use a single band model where spin-orbit interaction is ignored and carriers have angular momenta $J = 1/2$. Next, we introduce the spin-orbit coupling in a two-band model with $J = 3/2$. By changing the ratio of the masses of the light and heavy bands (m_l/m_h) we explore the effect of spin-orbit coupling. This is the minimal model that qualitatively captures the physics of DMS, however, a more realistic approach should incorporate the conduction and split-off bands and this will be discuss in future studies.

2.2 Model

We employ the simplified Hamiltonian proposed by Zaránd and Jankó[33] with an additional Coulomb potential term:

$$H = H_0 + J_c \sum_i \mathbf{S}(R_i) \cdot \mathbf{J}(R_i) + V \sum_i n(R_i), \tag{2.1}$$

where H_0 includes both electronic dispersion and spin-orbit coupling of the holes in the parent compound, J_c is the exchange coupling, V the Coulomb strength, $\mathbf{S}(R_i)$, $\mathbf{J}(R_i)$ and $n(R_i)$ are, respectively, the spin of the localized moment, the total angular momentum density and the density of the carriers at random site i. Short range direct or superexchange between Mn ions is ignored since we are in the dilute limit and we are not including clustering effects.

As discussed previously,[47, 48] within the DMFA the coarse-grained Green function matrix is:

$$\hat{G}(i\omega_n) = \frac{1}{N} \sum_k [i\omega_n \hat{I} - \hat{H}_0(k) + \mu \hat{I} - \hat{\Sigma}(i\omega_n)]^{-1}, \tag{2.2}$$

where N is the number of k points in the first Brillouin zone, μ the chemical potential, and $\hat{H}_0(k)$ and $\hat{\Sigma}(i\omega_n)$, are matrices representing the band structure of the parent material and the selfenergy, respectively. The mean field function $\hat{\mathcal{G}}_0(i\omega_n) = [\hat{G}^{-1}(i\omega_n) + \hat{\Sigma}(i\omega_n)]^{-1}$ is required to solve the DMFA impurity problem. At a non-magnetic site, the Green function is simply the mean field function $\hat{G}_{non}(i\omega_n) = \hat{\mathcal{G}}_0(i\omega_n)$. The Green function at a magnetic site is $\hat{G}_{\mathbf{S}}(i\omega_n) = [\hat{\mathcal{G}}_0^{-1}(i\omega_n) + J_c\mathbf{S}\cdot\hat{\mathbf{J}} + V]^{-1}$ for a given local spin configuration.

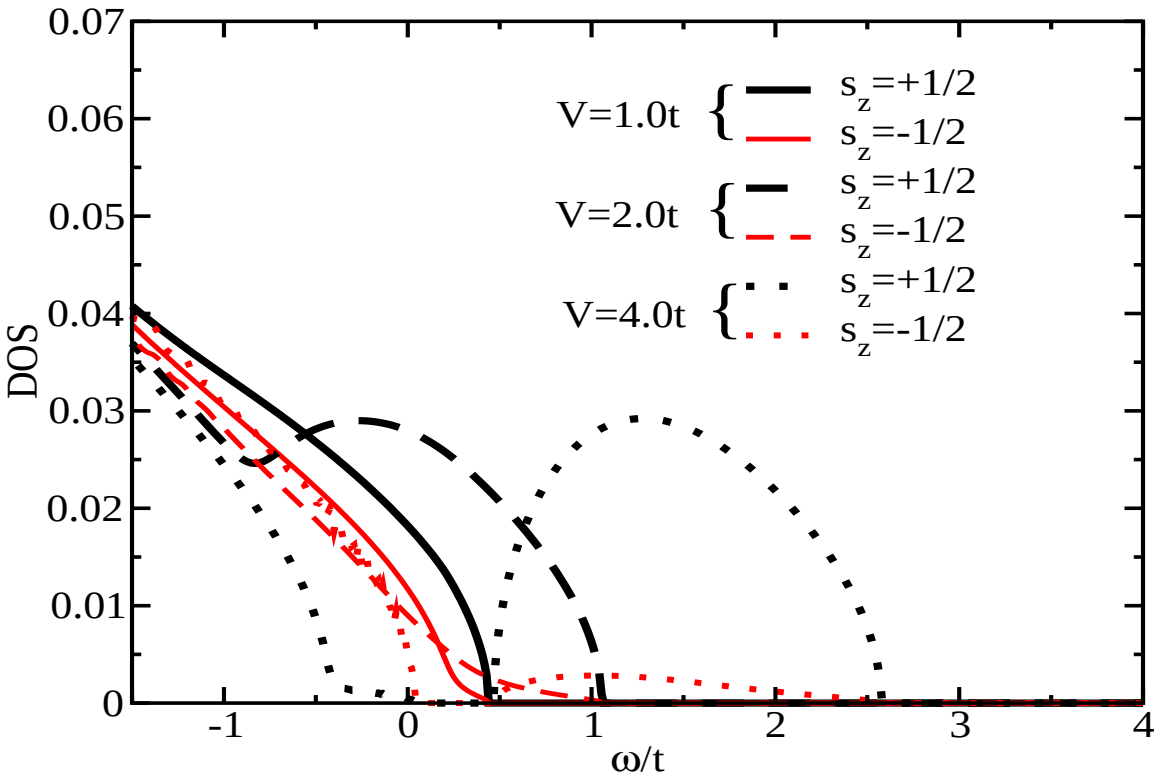

Figure 2.1: (Spin-dependent density of states for temperature T=0.01t, exchange coupling J_c=2t and Coulomb potential $V = 1\,t, 2\,t$ and $4\,t$. T=0.01t is below the ferromagnetic transition for all values of V.

Next we average $\hat{G}_{mag}$ over different spin orientation of the local moment. The relatively large magnitude of the Mn moment justifies a classical treatment of its spin. To get the average over the angular distribution we use the effective action [58, 59]

$$S_{eff}(\mathbf{S}) = -\sum_n \log\det[\hat{\mathcal{G}}_0^{-1}(i\omega_n) + J_c\mathbf{S}\cdot\hat{\mathbf{J}} + V]e^{i\omega_n 0^+}. \tag{2.3}$$

The average over spin configuration is

$$\langle\hat{G}_{mg}(i\omega_n)\rangle = \frac{1}{Z}\int d\Omega_{\mathrm{S}}\hat{G}_{\mathbf{S}}(i\omega_n)\exp[-\mathrm{S}_{\mathrm{eff}}(\mathbf{S})], \tag{2.4}$$

where Z is the partition function, $Z = \int d\Omega_{\mathbf{S}} \exp(-\mathrm{S}_{\mathrm{eff}}(\mathbf{S}))$. Finally the disorder is treated in a fashion similar to the coherent phase approximation (CPA)[55, 56, 57] and the averaged Green function reads $\hat{G}_{avg}(i\omega_n) = \langle \hat{G}_{mg} \rangle x + \hat{\mathcal{G}}_0(i\omega_n)(1-x)$ where x is the doping.

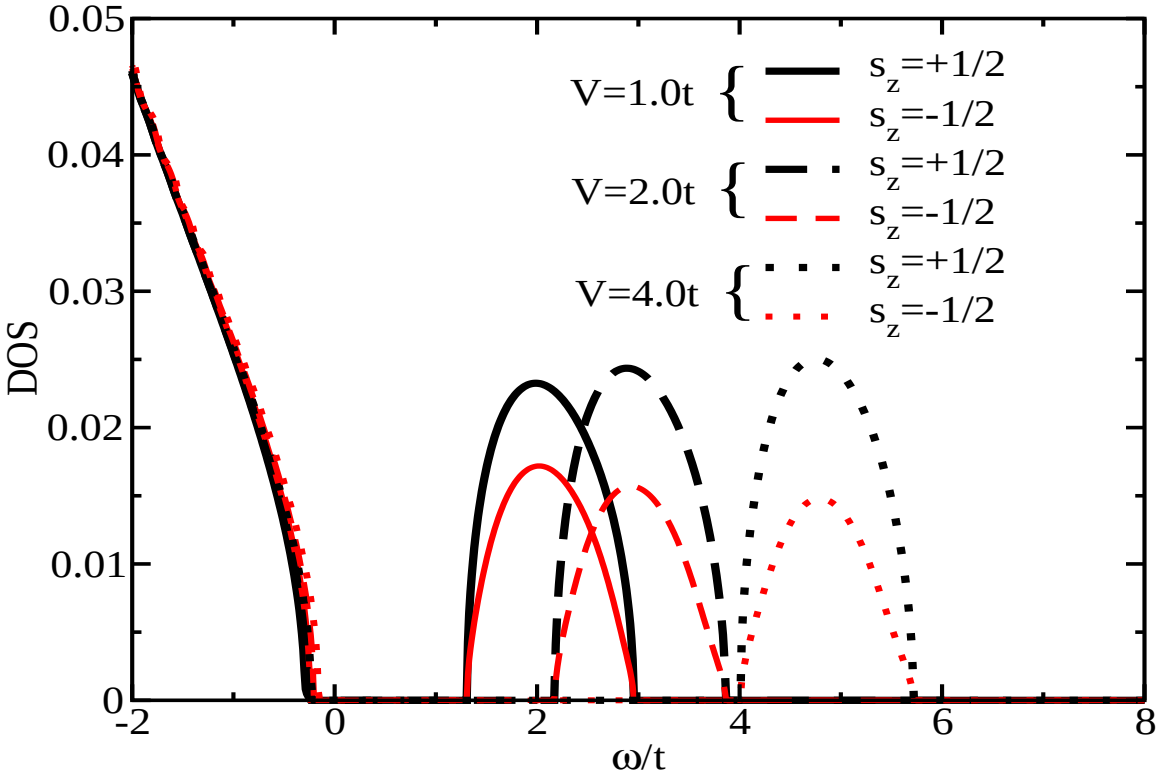

Figure 2.2: Spin-dependent density of states for temperature T=0.04t, exchange coupling J_c=5 t and various values of the Coulomb potential coupling V.

We obtain the hole density of states from the coarse-grained Green function in real frequency domain:

$$\hat{G}(\Omega) = \frac{1}{N} \sum_k [\Omega \hat{I} - \hat{H}_0(k) - \hat{\Sigma}(\Omega)]^{-1} \tag{2.5}$$

where $\Omega = \omega + i0^+$. The total density of states (DOS) is

$$DOS(\Omega) = -\frac{1}{\pi} \mathrm{Im} \mathrm{Tr} \hat{\mathrm{G}}(\Omega), \tag{2.6}$$

where Tr is the trace. Each diagonal element of the Green function $(-\frac{1}{\pi} Im\hat{G}(\Omega))$ corresponds to the density of states for a specific J_z component.

2.3 Results

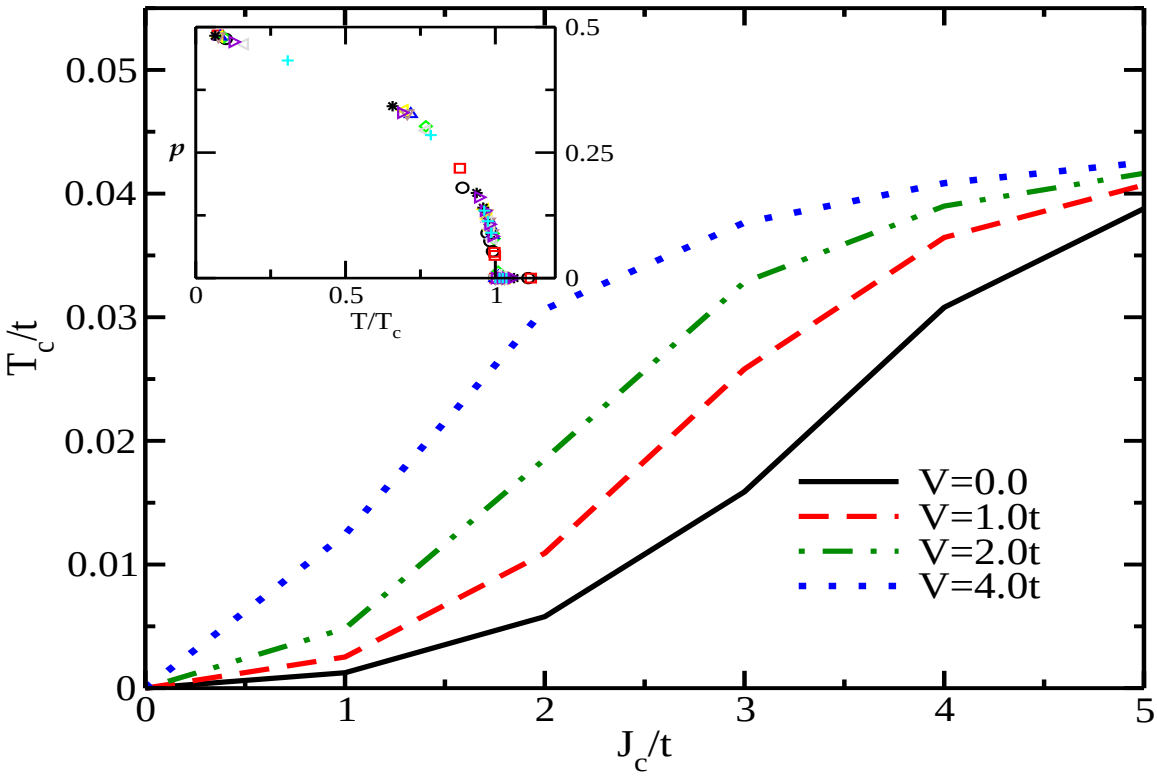

Figure 2.3: Ferromagnetic transition temperature versus magnetic exchange coupling for various values of the Coulomb potential. Inset: polarization of the holes as function of T/T_c for a wide range of values of J_c and V. Notice that all the polarization data collapse on a single curve.

Since $Ga_{1-x}Mn_xAs$ is grown using out of equilibrium techniques a noticeable fraction of manganese lies not on the Ga site (substitutional) but on the As site (anti-site) or somewhere in the middle of the crystal structure (interstitial)[20]. The real nature of interstitial defects is still controversial and yet to be resolved, [22, 21] but the one consensus is that in most samples there is strong compensation of the holes introduced by substitutional Mn. The density of carriers can also be controlled with electric fields.[60] We take these considerations into account by simply setting the filling of the holes to half of the nominal doping[49]. We focus on the doping x=5% and hole filling of $n_h = x/2$.

We start by discussing a simplified one-band model where we ignore the spin-orbit interaction. Our carrier dispersion is $\epsilon_k = -2t(\cos(k_x)+\cos(k_y)+\cos(k_z))$, where t is the spin independent hopping integral. Fig. 2.1 and 2.2 display the spin-dependent density of states (DOS) close to the edge of the valence band for coupling constant J_c=2 t and 5 t, respectively. Note that inclusion of the spin-independent attractive potential results

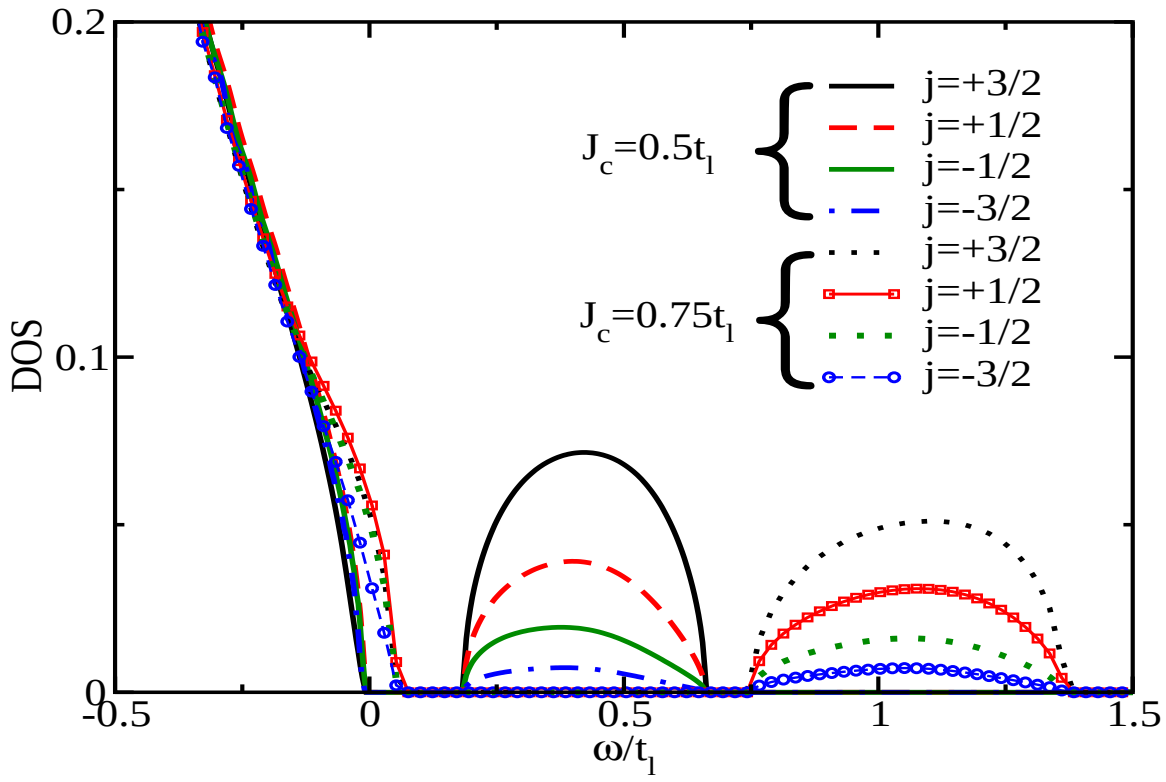

Figure 2.4: Density of states for V=0, and J_c =0.5 t_l, T=0.005 t_l; and 0.75 t_l at a temperature T=1/130 t_l. The impurity band is well formed with J_c=0.5t_l and increasing of the coupling shifts the impurity band to higher energies.

in shifting the energy of the holes (electrons) to lower (higher) energies for both spin species. This is in agreement with previous studies [50, 51]. Fig. 2.1 illustrates the strong influence of the Hartee term on the states close to the valence band edge for moderate exchange coupling. It is clear that increasing the Coulomb potential accelerates the formation of the impurity band and its splitting from the valence band. Fig. 2.2 shows that for couplings as large as J_c=5 t the impurity band is well formed even for relatively small Coulomb potentials (V=1 t) and the mere effect of the Coulomb term is to shift the impurity band. Notice also that the predicted shift of the impurity band is too large. We believe that this is a consequence of excluding the conduction band from our model, since band repulsion with the conduction band pushes the impurity band to lower energies.

The main panel in Fig. 2.3 shows the dependency of T_c on the exchange coupling for different Coulomb potentials within this simplified one-band model. Comparing this figure with Fig. 2.1 and 2.2 it is clear that T_c increases as impurity band forms and separates from the edge of the valence band. For each value of V we can identify two values of J_c for which the slope of the T_c vs. J_c curve changes. For $J_c < J_{min}$, T_c increases

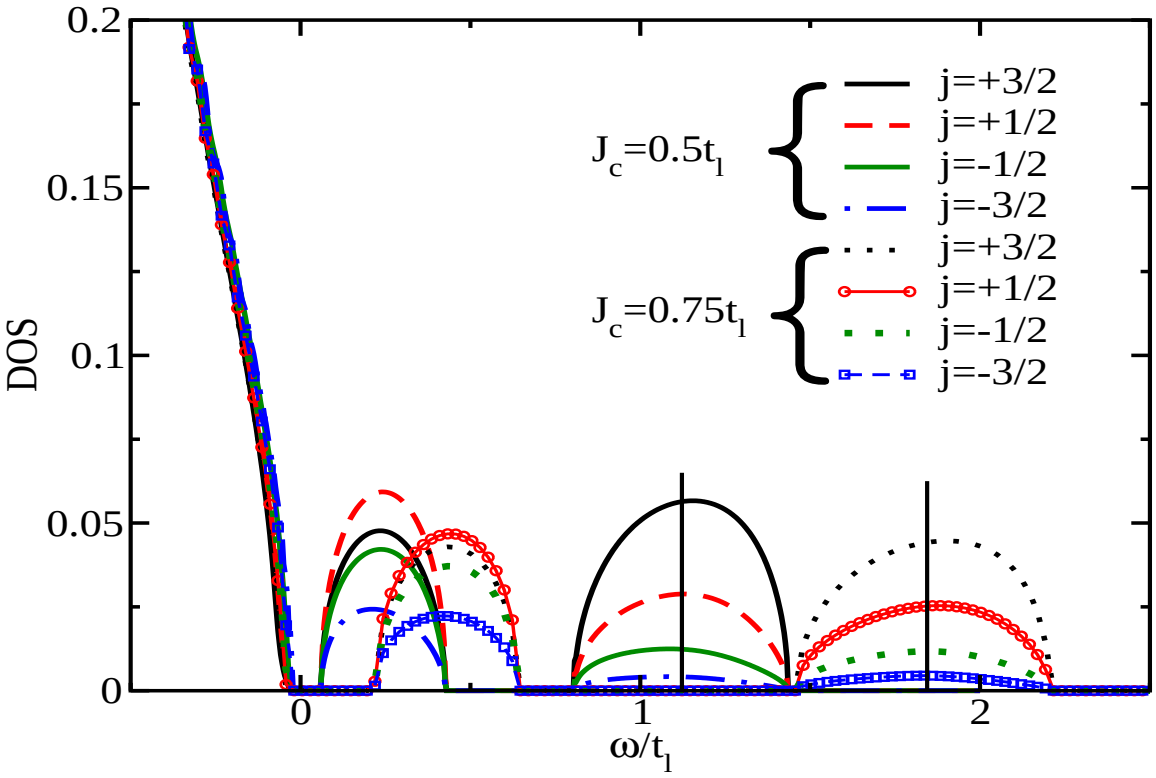

Figure 2.5: Density of states for $V = t_l$, J_c=0.5 t_l T=0.005 t_l; and 0.75 t_l at a temperature T=1/130 t_l. The attractive potential enhances the formation of the impurity band as compared with Fig. 2.4. The chemical potential lies in the middle of the first impurity band, as it is displayed by the vertical black line.

very slowly, for $J_{min} < J_c < J_{sat}$ the impurity band begins to develop and T_c increases with the largest slope, for $J_c > J_{sat}$ the impurity band is completely split from the valence band and the rate of increase in T_c reduces dramatically. In brief, the appearance of the impurity band corresponds to the large change in the curvature of T_c vs. J_c. After the impurity band is well formed increasing J_c or V does not change T_c significantly. In fact, for $J_c > 4\,t$ we can anticipate the saturation of the critical temperature. This is an artifact of the DMFA and is due to the absence of non-local correlations. Inclusion of those correlations leads to magnetic frustration of the system, which in turn suppresses T_c.[61, 33] We will come back to this point in more detail later when we discuss the two-band model.

Therefore by increasing the attractive Coulomb potential T_c is significantly enhanced for values of the exchange in a given interval, $J_{min}(V) < J_c < J_{sat}(V)$, where $J_{min}(V)$ and $J_{sat}(V)$ are function of V. This is due mostly to the fact that a positive V promote the appearance of localized states at the magnetic sites which mediate the magnetic order. However, the physics of the ferromagnetic state is not modified by V, since the only relevant energy scale is given by T_c, as one expects from a mean field theory. This is illustrated

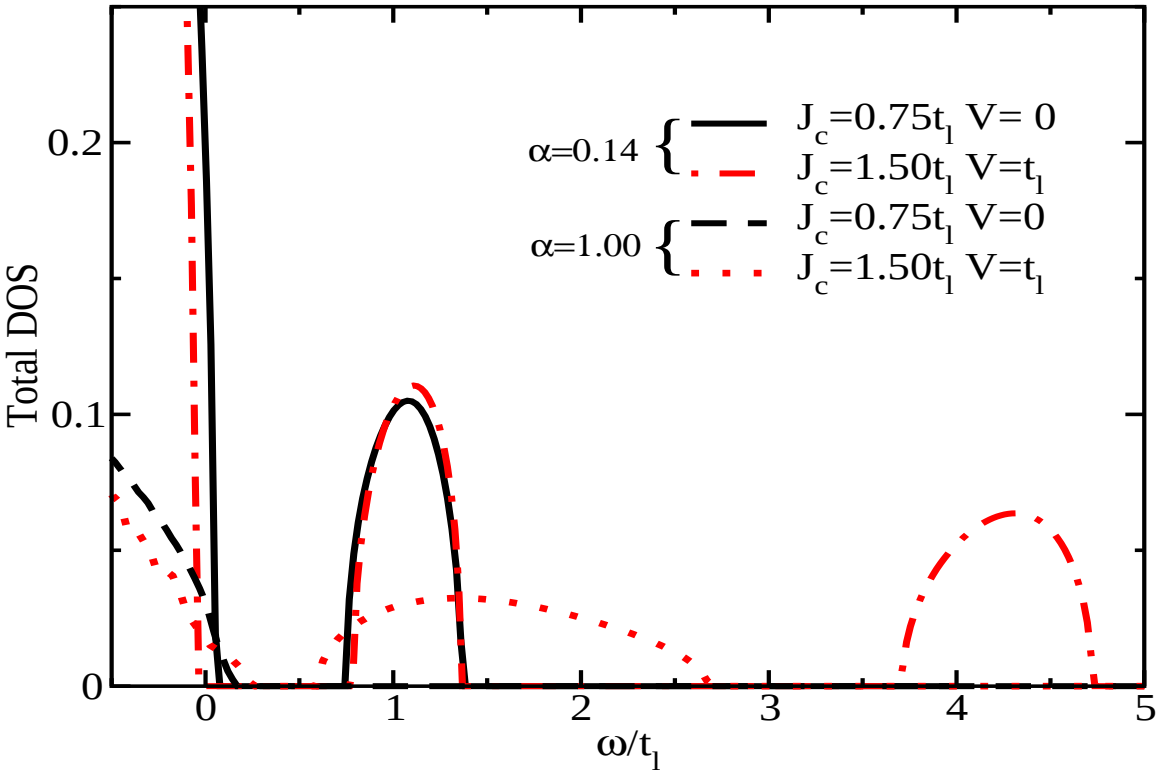

Figure 2.6: Density of states for two values of the exchange coupling and Coulomb term: $J_c = 0.75\,t_l$, $V = 0$ and $J_c = 1.5\,t_l$, $V = t_l$, and temperatures well bellow the ferromagnetic transition, for α=0.14 and 1.0.

in the inset of Fig. 2.3 that displays the polarization of the holes as function of T/T_c for a wide range of values of J_c and V, showing that all the polarization data collapse on a single curve. Thus, the effect of V is just to change the nominal value of J_c to a larger J_c^{eff}.

Now, we introduce a more realistic approach using a two-band model. The spin-orbit interaction and the crystal fields lift the degeneracy of the p-like valence bands into heavy, light and split-off bands. In our model we ignore the effect of the split-off band and focus on the heavy and light bands which are degenerate at the center of the Brillouin zone.[34] H_0 is approximated by $H_0(k) = \hat{R}^{\dagger}(\hat{k})\hat{\epsilon}(k)\hat{R}(\hat{k})$, where $\hat{\epsilon}(k)$ is a diagonal matrix with entries $\epsilon(k)_{n,\sigma} = -2t_n(\cos(\mathrm{k_x}) + \cos(\mathrm{k_y}) + \cos(\mathrm{k_z}))$, with $n = l, h$ the heavy/light band index and $\hat{R}(\hat{k})$, the $k \cdot p$ spin 3/2 rotation matrices.[47] In GaAs the mass ratio of light and heavy holes at the Γ point is $\alpha = m_l/m_h = 0.14$ [62]. We compare the results of our simulation for α=0.14 and α=1, keeping the bandwidth of the light hole band fixed. Furthermore we scale every parameter according to the light holes hopping energy (t_l), which set the bandwith of the hole band.

Fig. 2.4 displays the hole density of states close to the edge of the valence band for J_c= 0.5 t_l and 0.75 t_l in absence of the Coulomb potential, and for temperatures well below the ferromagnetic transition temperature.

One can anticipate that the formation and splitting of the impurity band happens for smaller values of J_c/t_l than in the one-band model. We can explain this by noting that the total angular momentum of the holes can be as large as J=3/2 for heavy holes, leading to a larger contribution to the total energy from the the second term in Eq. (5.1). Moreover, for a small filling there are more available states close to the center of the Brillouin zone in the two-band model than in the one-band model. Larger number of spin states available to align along the direction of the local moment increases the average exchange energy and favor ferromagnetism.

Fig. 2.5 displays the density of states for the same exchange couplings and temperatures, J_c= $0.5\,t_l$, T=$0.005\,\mathrm{t}_l$, and $0.75\,t_l$, T=$1/130\,\mathrm{t}_l$, but with a finite Coulomb potential V=t_l. For these values of the parameters a second impurity band appears in the semiconducting gap. The appearance of two impurity bands is consistent with the fact that the model includes two bands with $J_z = \pm 3/2, \pm 1/2$. Notice that the second impurity band is more populated with light holes ($J_z = 1/2$) while the first impurity band, with higher energy, is mostly made of heavy holes ($J_z = 3/2$). Since we keep the filling of the holes fixed (n_h=$x/2$) the chemical potential sits in the middle of the first impurity band, as shown in Fig. 2.5. Thus, as we discussed previoulsy, the shift of the impurity band will not have noticeable effects on the magnetic properties of the DMS.

To investigate the effect of the spin-orbit interaction we introduce a simple toy model which has all the features of our two-band model except that the heavy and light bands are degenerate over the whole Brillouin zone. Therefore, heavy and light bands have the same dispersion but different total angular momenta j_z=$\pm 3/2$ and $\pm 1/2$, respectively. The different band masses introduce magnetic frustration[33, 49] and by setting α=1.0 (m_h=m_l) in our model, this magnetic frustration is removed. Since t_l is fixed, changes in α alters the dispersion of the heavy hole band while keeping the light band fixed.

Fig. 2.6 displays the total DOS for two values of the exchange coupling and Coulomb potential: J_c = $0.75\,t_l$, $V = 0$ and $J_c = 1.5\,t_l$, $V = t_l$, and for α=0.14 and 1.0. Note that for α=0.14 the impurity band is formed at lower couplings. Thus, the spin-orbit interaction enhances the formation of the impurity band. We can explain this by noting that changing α from 1.0 to 0.14 decreases the kinetic energy of the heavy holes (with j_z=3/2) becoming more susceptible to align their spin parallel to the local moment promoting the formation of the impurity band. Fig. 2.4 and 2.5 show explictly that the heavy holes are the majority of the carriers in the impurity band. On the other hand the bandwidth of the impurity band is larger when α=1.0, pointing to less localized holes, which better mediate the exchange interaction between magnetic ions.

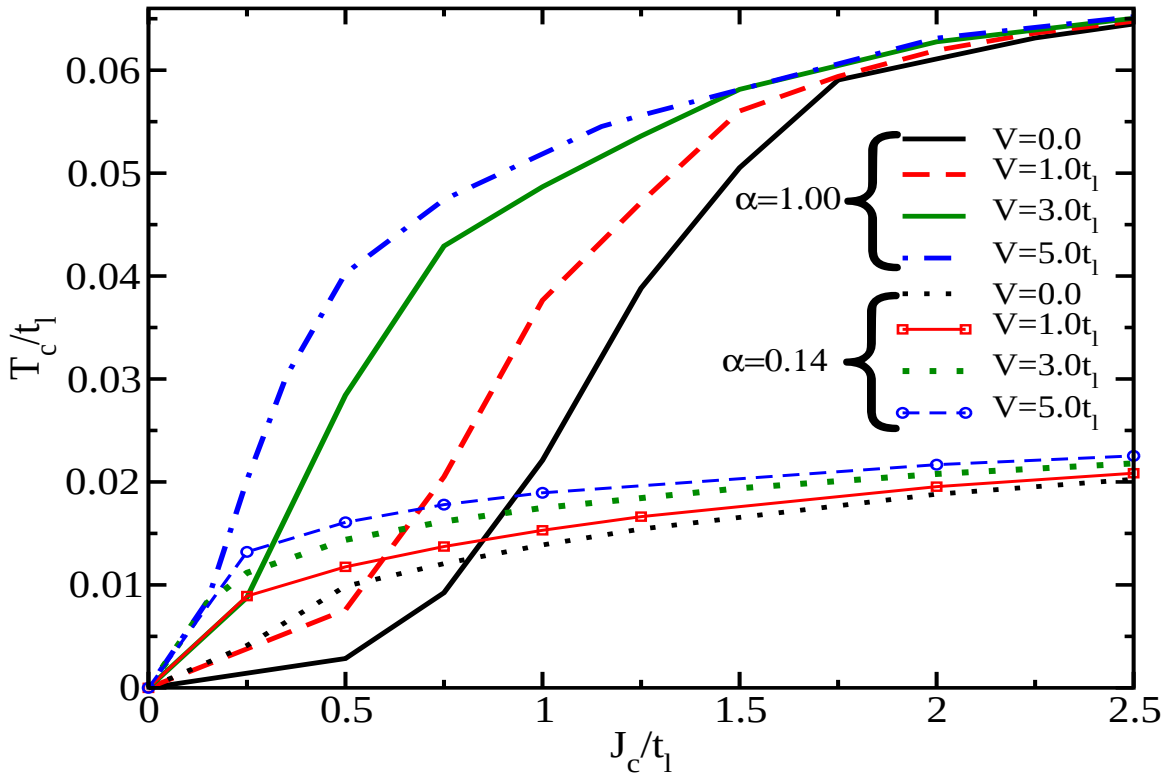

Figure 2.7: Ferromagnetic transition temperature, T_c, vs. exchange coupling J_c, both in units of t_l, for different values of the Coulomb potential and for α=0.14 and 1.0.

Finally we look at the dependence of the critical temperature on the parameters of the model: J_c, V and α. The results for different values of J_c-V for α=1.0 and 0.14 are shown in Fig. 2.7. Similarly to Fig. 2.3 we can identify for both values of α a range of parameters J_c, V where T_c increases strongly. This corresponds to the formation and splitting of the impurity band from the valence band. For small values of J_c and V, T_c is higher for $\alpha = 0.14$ but as we increase J_c-V the ferromagnetic transition temperature for $\alpha = 1.0$ becomes larger. Eventually T_c saturates due to the lack of non-local correlations within the DMFA. We can understand the higher T_c for $\alpha = 0.14$ and small J_c,V by looking at Fig. 2.6. For $\alpha = 0.14$ the impurity band appears at smaller values of J_c and V than for $\alpha = 1.0$. This is due to the fact that the heavy holes have a smaller kinetic energy and can be polarized more easily and become bonded to the localized moments forming the impurity band. For larger values of J_c and V, $J_c > 0.81t_l$ for $V = 0$, $J_c > 0.60t_l$ for $V = 1\,t_l$ or $J_c > 0.29t_l$ for $V = 3\,t_l$, the critical temperature for the model with α=1.0 surpasses the one for α=0.14 in agreement with previous findings in the strong coupling regime[47, 49]. This also can be related with the DOS in Fig. 2.6, where the bandwith of the impurity band for α=1.0 is larger than for α=0.14. A larger bandwidth corresponds to weaker localization of the holes and higher mobility. Therefore, they will

better mediate the ferromagnetic interaction between the magnetic ions and we expect to see higher T_c when $\alpha = 1.0$. For the largest value of J_c and V we study $T_c(\alpha = 0.14)/T_c(\alpha = 1.) = 0.35$ to compare with 0.48 obtained in the strong coupling limit[49].

2.4 Conclusions

In conclusion, we have calculated densities of states, polarizations and ferromagnetic transition temperatures for a one-band and two-band models appropriate for $Ga_{1-x}Mn_xAs$. We have investigated the effect of adding a local Coulomb attractive potential V between the magnetic ions and the charge carriers. The inclusion of a Coulomb term leads to the formation of the impurity band for smaller magnetic couplings (J_c), in agreement with previous studies[50, 51] and it significantly enhances T_c for a wide range of J_c, without affecting the intrinsic physics of the ferromagnetic transition. We also explore the effect of the spin-orbit interaction by using a two-band model and two different values of the ratio of the effective masses of the heavy and light holes. We show that in the regime of small J_c-V the spin-orbit interaction enhances T_c, while for large enough values of J_c-V the magnetic frustration induced by the spin-orbit coupling reduces T_c to values comparable to the previously calculated strong coupling limit.

Chapter 3

Nonlocal Effects on Magnetism in the Diluted Magnetic Semiconductor $Ga_{1-x}Mn_xAs$

3.1 Introduction

The discovery of high temperature ferromagnetism in diluted magnetic semiconductors (DMS) has stimulated a great deal of attention [11]. The interest in these materials is due to possible applications in spintronics [63] as the source of a spin polarized current or as the base material for a chip that can simultaneously store and process data.

In spite of extensive studies, our understanding of ferromagnetism in these systems is far from complete [20]. There are a few serious difficulties in the theoretical study of DMS: (i) The magnetic interaction between local magnetic moments and itinerant carrier spin, which is responsible for the high transition temperature (T_c), is strong and outside the Ruderman-Kittel-Kasuya-Yosida (RKKY) regime. (ii) There exists strong disorder from the random distribution of magnetic ions. (iii) Nonlocal effects are expected to be crucial judging from the spatially oscillating and anisotropic magnetic interaction predicted in theory [33, 49, 64, 65] and observed in experiments [66].

The mean-field study by Dietl *et al.* [67] captures the main features of DMS systems qualitatively and some even quantitatively. However, it ignores strong correlations, disorder effects, and spatial fluctuations, and fails to describe some DMS materials, such that subsequent studies have brought their approach into question [68, 69]. Studies [70, 71, 47, 72] based on the dynamical mean-field theory (DMFT) [43, 73] have made considerable improvements by including strong correlation and disorder effects. However, the local nature of the DMFT presents severe limitations when studying this system. The effects of short-range fluctuations and spatial correlations were shown to be important in the classical Heisenberg model [14]. In this chapter, we show that nonlocal effects may be equally important for the itinerant carriers, which mediate the effective interaction between local moments in DMS. The dynamical cluster approximation (DCA) [74] systematically incorporates nonlocal effects as the cluster size (N_c) increases while retaining

This work has been published in Phys. Rev. Lett., **104** , 037201 (2010)

strong correlations. When $N_c = 1$, the DCA is equivalent to the DMFT, and exact results are approached as $N_c \to \infty$. Since all the possible disorder configurations are considered in a cluster, the DCA is also a better approximation for disorder average than the coherent potential approximation or DMFT by including multi-impurity scattering terms [75, 76]. Thus, the DCA is an ideal method for studying DMS systems. In this chapter, we study the magnetic properties of the prototypical DMS system $Ga_{1-x}Mn_xAs$ using the DCA and the $\mathbf{k}\cdot\mathbf{p}$ method, which describes the non-interacting band structure of pure GaAs. We show that nonlocal effects are very important for properly capturing the magnitude of T_c, the saturation magnetization, and the magnetic anisotropy of this material. In particular, we show that the strong cluster anisotropy is responsible for the magnetic anisotropy along the cube-edge direction and the spin reorientation at low temperature.

3.2 Method

The model Hamiltonian we adopt is

$$H = H_{\mathbf{k}\cdot\mathbf{p}} + J_c \sum_I \mathbf{S}(R_I)\cdot\mathbf{J}(R_I), \tag{3.1}$$

where the first term describes the electronic structure of the host material (GaAs) in the $\mathbf{k}\cdot\mathbf{p}$ approximation and the second term introduces a magnetic interaction between the carrier spin ($\mathbf{J}$) and the local magnetic moment ($\mathbf{S}$) of Mn at position R_I. The large magnitude of the Mn magnetic moment ($S = 5/2$) allows us to treat it classically. This model is generally accepted to describe DMS [33, 49, 67, 70, 71, 47, 72, 77, 78], since a mean-field treatment of the Hamiltonian [67, 77, 78] is able to explain many physical properties of the system. For the $\mathbf{k}\cdot\mathbf{p}$ Hamiltonian ($H_{\mathbf{k}\cdot\mathbf{p}}$), we adopt a 4×4 Luttinger-Kohn model describing heavy and light hole bands with spin-orbit coupling, but ignoring the conduction and split-off bands. We use the Luttinger parameters $\gamma_1 = 6.98$, $\gamma_2 = 2.06$, and $\gamma_3 = 2.93$ [79]. Biaxial strain is included in $H_{\mathbf{k}\cdot\mathbf{p}}$ through the strain tensor $\varepsilon_{xx} = \varepsilon_{yy} = \varepsilon_0 = \Delta a/a$ and $\varepsilon_{zz} = (-2c_{12}/c_{11})\varepsilon_0$ with the ratio of elastic stiffness constants $c_{12}/c_{11} = 0.46$. Parameter a is the lattice constant of $Ga_{1-x}Mn_xAs$, and Δa is the difference between the lattice constants of $Ga_{1-x}Mn_xAs$ and the substrate. We use the hydrostatic deformation potential $a_v = 1.16$ eV and the shear deformation potential $b = -2.0$ eV [79].

In addition to the parameters of the $\mathbf{k}\cdot\mathbf{p}$ Hamiltonian, we must determine the value of the exchange coupling J_c. It can be obtained from photoemission [80], infrared [81, 82], and resonant tunneling [83] spectroscopy and magneto-transport experiments [84], which give J_c = 0.6-1.5 eV. We adopt $J_c = 1$ eV throughout this chapter.

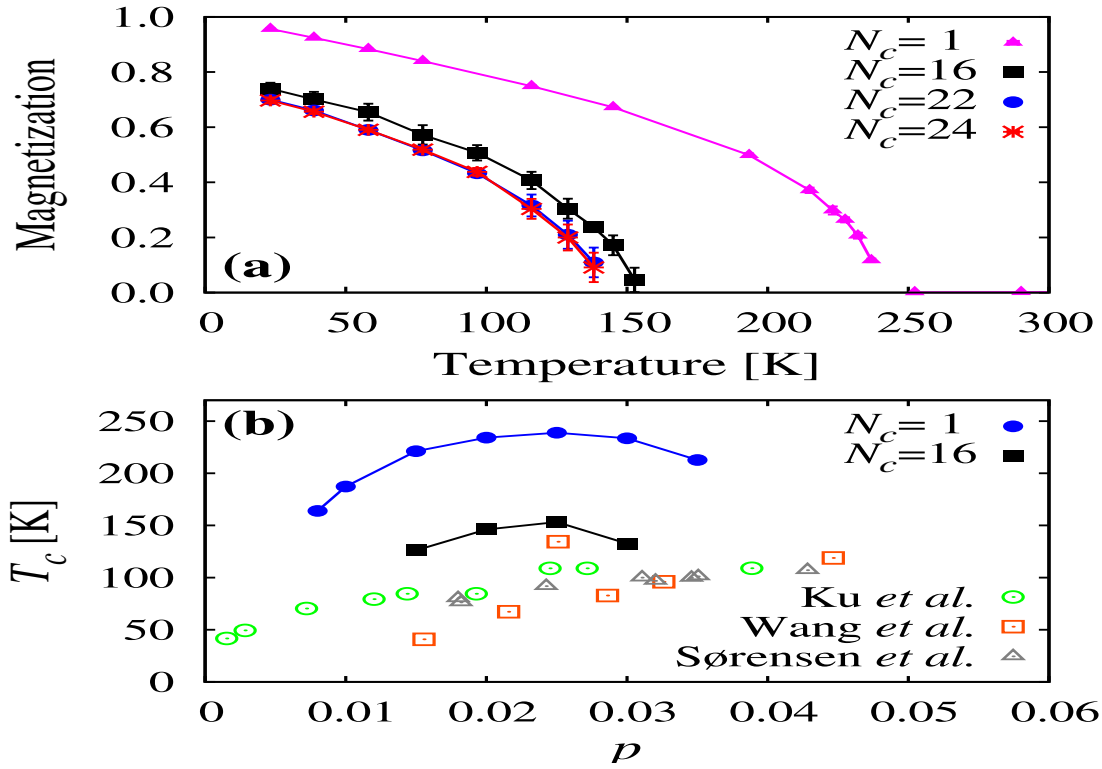

Figure 3.1: (a) Magnetization of $Ga_{1-x}Mn_xAs$ calculated by DMFT ($N_c = 1$) and DCA ($N_c = 16$, $N_c = 22$, and $N_c = 24$) with Mn doping $x = 0.05$ and hole concentration $p = 0.025$. No strain effect is considered. (b) Ferromagnetic transition temperature (T_c) as a function of hole concentration (p) with DMFT ($N_c = 1$) and DCA ($N_c = 16$) for $x = 0.05$. Experimental results [1, 2, 3] are also shown. The Mn concentration in experiments is x=0.085 (Ku *et al.*), x=0.017-0.09 (Wang *et al.*), and x=0.05 (Sørensen *et al.*).

Figure 3.1(a) shows the magnetization per Mn ion of the $Ga_{1-x}Mn_xAs$ system as a function of temperature with DMFT ($N_c = 1$) and DCA ($N_c = 16$, $N_c = 22$, and $N_c = 24$). We chose three fcc clusters that are *perfect* according to Betts *et al.* [85]. The difference between DCA and DMFT stems from nonlocal effects, not captured in DMFT. The T_c with DCA is far lower than that obtained with DMFT, approaching the regime of experimental values [1, 2, 3] [see Fig. 3.1(b)]. Another important point is the reduction of the saturation magnetization at low temperature, consistent with experiments [3, 86, 87]. This behavior is a product of the rotational frustration [33], to be discussed in detail later. This effect also reduces T_c. The dependence of T_c on hole concentration (p) is shown in Fig. 3.1(b). T_c attains a maximum value when hole concentration is half of Mn concentration, consistent with previous DMFT studies [70, 71, 47, 72].

Next, we studied the magnetic anisotropy of $Ga_{1-x}Mn_xAs$. The magnetic anisotropy of this system depends on strain, hole concentration, and temperature in a complicated manner, but generally it has in-plane anisotropy with compressive strain and perpendicular-to-plane anisotropy with tensile strain [11]. With

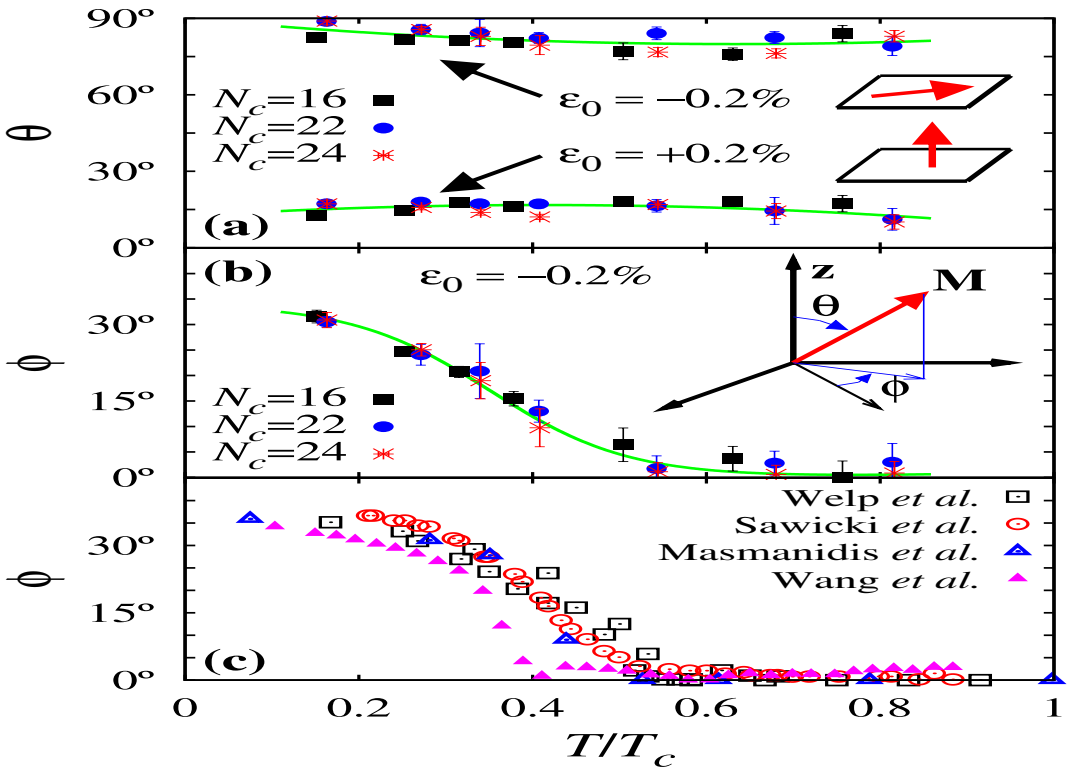

Figure 3.2: (a) Polar angle (θ) of the magnetization as a function of the normalized temperature (T/T_c) for two strain values. Compressive ($\varepsilon_0 = -0.2\%$) and tensile ($\varepsilon_0 = +0.2\%$) strain induce in-plane and perpendicular magnetic anisotropy, respectively. (b) Azimuthal angle (ϕ) of the magnetization with respect to the [110] direction with compressive strain. Experimental results [4, 5, 6, 7] are provided in (c) to compare with (b).

compressive strain, the magnetization changes direction within plane from [110] or [1$\bar{1}$0] at high temperature to [100] or [010] at low temperature [4, 5, 6, 7] [see Fig. 3.2(c)]. As is shown in Fig. 3.2(a) and 3.2(b), the DCA reproduces experimental results on the dependence of magnetic anisotropy on strain and temperature remarkably well.

While the strain dependence of the magnetic anisotropy was explained within the mean-field theory [77, 78], the spin reorientation within the plane has not been explained yet. In the absence of strain, $Ga_{1-x}Mn_xAs$ has diagonal magnetic anisotropy within the mean-field theory because the heavy holes, which dominate at low carrier density, have larger density along the diagonal direction in **k**-space [77]. With compressive strain, it has the anisotropy in [110] or [1$\bar{1}$0]. This explains the magnetic anisotropy at high temperature.

The [100] or [010] anisotropy at low temperature is due to the cluster anisotropy originating from the anisotropic interaction between neighboring Mn ions. Because Mn ions are distributed randomly throughout

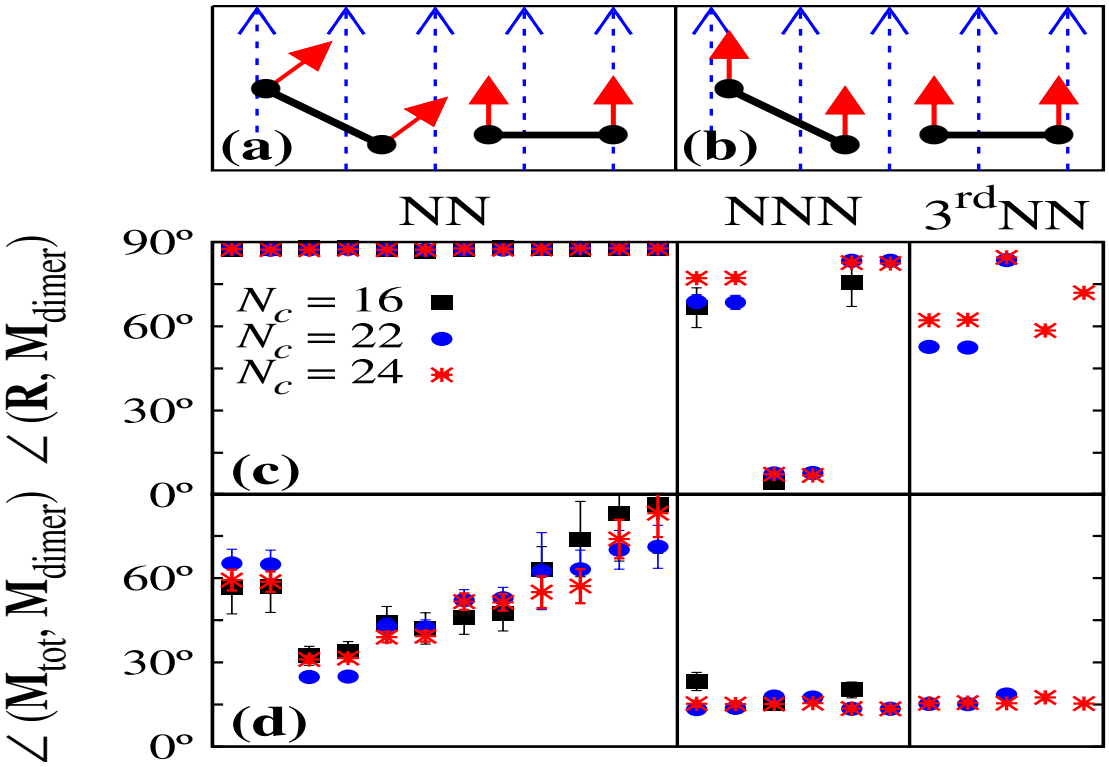

Figure 3.3: (a) DCA results at low temperature show that the dimer magnetization ($\mathbf{M}_{\rm dimer}$) is prefered to be perpendicular to the vector connecting the two Mn ions ($\mathbf{R}$) for nearest-neighbor (NN) Mn-dimers. (b) For larger dimers, $\mathbf{M}_{\rm dimer}$ aligns with the total magnetization ($\mathbf{M}_{\rm tot}$) irrespective of $\mathbf{R}$. The dotted and solid arrows represent $\mathbf{M}_{\rm tot}$ and $\mathbf{M}_{\rm dimer}$, respectively. (c) and (d) Angle between $\mathbf{M}_{\rm dimer}$ and $\mathbf{R}$ and between $\mathbf{M}_{\rm dimer}$ and $\mathbf{M}_{\rm tot}$, respectively, at T=23.2 K, x=0.05, p=0.025, and ε_0=−0.2%. The left panel is for the 12 NN dimers [*e.g.*, when the two Mn ions are at $(0,0,0)$ and $(a/2,a/2,0)$], the middle panel is for the 6 next-nearest-neighbor (NNN) dimers [*e.g.*, when the two Mn ions are at $(0,0,0)$ and $(a,0,0)$], and the right panel is for the third-nearest-neighbor ($3^{\rm rd}$NN) dimers [*e.g.*, when the two Mn ions are at $(0,0,0)$ and $(a,a/2,a/2)$].

the system, the number of Mn ions within a cluster varies between zero and N_c. We call a cluster a monomer (dimer) when it includes one Mn ion (two Mn ions). All possible distributions of Mn ions are considered effectively in this calculation, but at low doping, the magnetic properties are dominated by Mn-monomers and Mn-dimers. Since there is no cluster anisotropy in monomers, we investigate magnetization of Mn-dimers in detail. Because of translational symmetry, we need to consider only $N_c - 1$ dimers. The two Mn ions are nearest-neighbors in 12 dimers, next-nearest-neighbors in 6 dimers, and third-nearest-neighbors in $N_c - 19$ dimers. Figure 3.3 shows the magnetization direction of each dimer obtained by the Monte-Carlo method at low temperature. The magnetization of the nearest-neighbor Mn-dimer is always perpendicular to the vector connecting the two Mn ions. This cluster anisotropy prevents the magnetic moment of some dimers from aligning parallel to the total magnetization and leads to the rotational frustration [33, 49]. When the

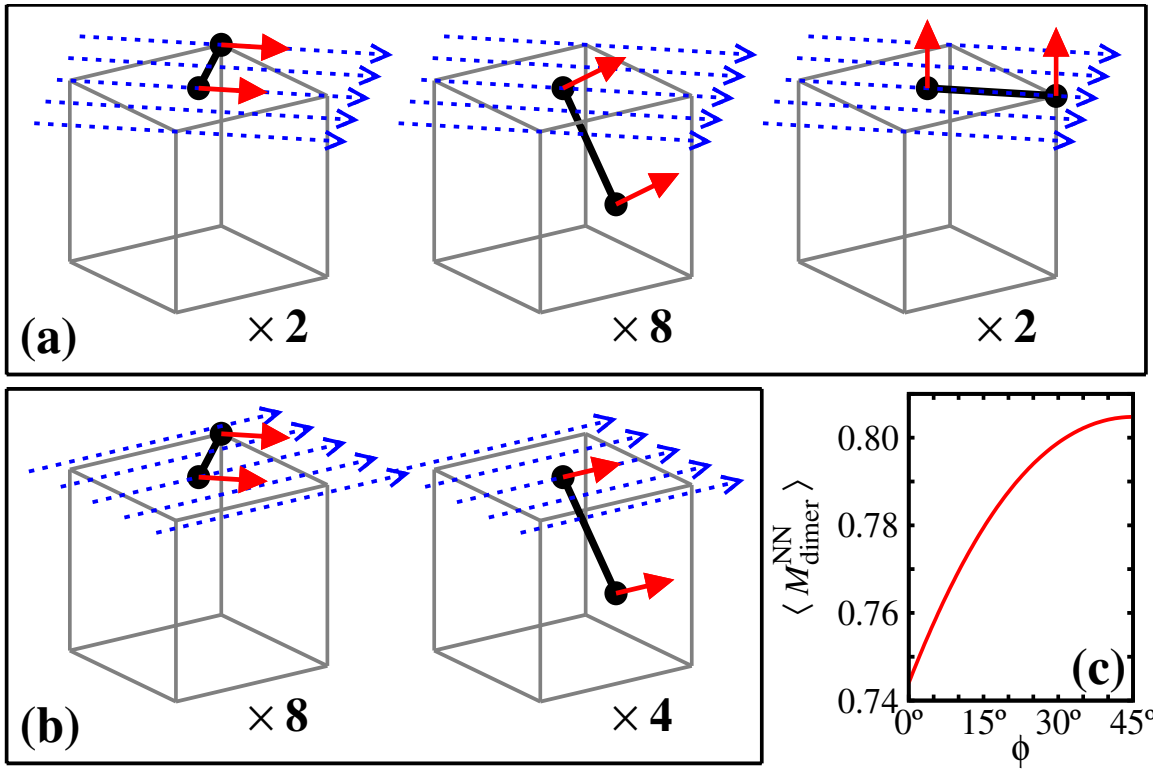

Figure 3.4: (a) Magnetic configurations of the 12 nearest-neighbor (NN) Mn-dimers ($\mathbf{M}^{\rm NN}_{\rm dimer}$) that maximize the total magnetization ($\mathbf{M}_{\rm tot}$) when $\phi = 0°$ (*i.e.* $\mathbf{M}_{\rm tot}$ is along [110] or [1$\bar{1}$0]). The dotted and solid arrows represent $\mathbf{M}_{\rm tot}$ and $\mathbf{M}^{\rm NN}_{\rm dimer}$, respectively. The numbers below each diagram indicate the degeneracy of the Mn-dimer configurations. The dimer configuration with $\mathbf{M}^{\rm NN}_{\rm dimer}$ perpendicular to the vector connecting the two Mn ions ($\mathbf{R}$) is energetically favored. (b) Same as (a) but when $\phi = 45°$ (*i.e.* $\mathbf{M}_{\rm tot}$ is along [100] or [010]). (c) Maximum value of the average $\mathbf{M}^{\rm NN}_{\rm dimer}$ vs. ϕ .

two Mn ions are farther apart, this anisotropy is very weak and magnetization of the dimer aligns parallel to the total magnetization.

The cluster anisotropy can also explain the enhancement of T_c up to 260 K in the quasi-two-dimensional δ-doped systems [17]. When the Mn ions are within one plane, all the nearest-neighbor Mn-dimers can point in the same direction (perpendicular-to-plane direction) without rotational frustration. This may induce a larger saturation magnetization and higher T_c in these systems.

Notably, due to this cluster anisotropy, the maximum total magnetization depends on the magnetization direction, and this dependence introduces another type of magnetic anisotropy. When we assume the magnetic moment is perpendicular to the vector connecting the two Mn ions and in-plane magnetization, the maximum value of the average magnetization of the 12 nearest-neighbor dimers is calculated to be

$$\langle M^{\rm NN}_{\rm dimer} \rangle \quad = \quad \frac{1}{6}\left[\cos\phi + \sin\phi + \sqrt{3 + \sin(2\phi)}\right.$$

$$+\sqrt{3-\sin(2\phi)}\Big] \tag{3.2}$$

for the fcc lattice. This becomes maximal when the magnetization is along [100] or [010], as shown in Fig. 3.4(c). Since larger magnetization leads to lower magnetic energy, it introduces magnetic anisotropy along [100] or [010]. We note that this effect becomes unimportant at high temperature, where the total magnetization is small. Thus, the spin reorientation from [110] or $[1\bar{1}0]$ at high temperature to [100] or [010] at low temperature is captured within our calculation. This behavior arises from the multi-impurity scattering and cannot be obtained within the mean-field theory or the DMFT.

In summary, we investigated the magnetic properties of the prototypical DMS system $Ga_{1-x}Mn_xAs$ by DCA together with the $\mathbf{k}\cdot\mathbf{p}$ method. We showed that nonlocal effects, not included in the mean-field theory or the DMFT but included in the DCA for $N_c > 1$, are very important to quantitatively explain the T_c, the saturation magnetization, and the magnetic anisotropy of this material. We find that the edge-direction anisotropy at low temperature is due to the cluster anisotropy, and this allows us to reproduce the spin reorientation in this system remarkably well.

Chapter 4

Dynamical Mean Field Approximation of a Tight-binding Model of $Ga_{1-x}Mn_xAs$

4.1 Introduction

The discovery of a new generation of dilute magnetic semiconductors (DMS) with large Curie temperature [11, 13] has led to numerous experimental and theoretical studies.[67, 20] The ultimate goal is to find a DMS with ferromagnetic transition about room temperature to use in spintronic devices. One of the most promising candidates is $Ga_{1-x}Mn_xAs$ due to its rather high T_c, [67, 11] and compatibility with current electronic applications. Despite this huge interest, some of the most basic questions about $Ga_{1-x}Mn_xAs$ are still unanswered after more than a decade of its discovery. Among them are questions about the nature of its underlying magnetic interactions and the role of the impurity band.

In this work we combine the sp^3 tight-binding Hamiltonian for the zincblende GaAs with the self consistent dynamical mean field approximation (DMFA) to study the magnetic and transport properties of $Ga_{1-x}Mn_xAs$. We suppose that the manganese (Mn) doping does not modify the tight-binding parameters of GaAs and any change in the band structure is due to the many-body effects induced by the magnetic coupling between the Mn local moments and the itinerant holes.

Several previous studies have used the tight-binding approximation for DMS. Tang and Flatté calculated the local density of states for a single Mn and two nearby Mn impurities[88] and the magnetic circular dichroism[89] of bulk $Ga_{1-x}Mn_xAs$ using large supercells; Masek *et al.* took the Weiss mean field approach to calculate the electronic structure for several DMS[90]; and Turek *et al.* compared both tight-binding approaches results[91, 92]. Large-scale Monte Carlo studies of real-space tigh-binding Hamiltonians including only the three valence bands has also been performed [93]

Our DMFA calculation includes quantum self-energy corrections which are not included in other mean-field theories. We also incorporate valence and conduction bands on an equal footing. Because this method is non-perturbative, it allows us to study both the metallic and impurity-band regimes as well as small and large couplings. Since the coupling between the magnetic ions and charge carriers is comparable to

the Fermi energy, temporal fluctuations must be included in a realistic calculations specially in the vicinity of the critical temperature. We choose tight-binding parameters according to Chadi and Cohen [94, 95], which give the correct features of GaAs within the relevant energy scale around the Fermi energy, such as effective masses for valence and conduction bands and the gap at the center of the Brillouin zone. Our model also includes the spin-orbit interaction of the parent material which was proved very important in previous studies[33, 49, 96] of $Ga_{1-x}Mn_xAs$. The inclusion of the realistic band structure of the parent material leads to more realistic results. For example, the band repulsion between the conduction band and the impurity band, which was absent in previous calculations based on the $k \cdot p$ approach [47, 96, 48] results in a significant reduction of the bandwidth of the impurity band . Narrowing of the impurity bandwidth corresponds to the localization of the mediating holes which ultimately suppresses the previously overestimated critical temperature. We find that the calculated T_c is significantly smaller (and closer to the experimental results) by improving the band structure of the parent compound.

4.2 Model

We model the magnetic interactions in $Ga_{1-x}Mn_xAs$ using the simplified Hamiltonian proposed by Zaránd and Jankó[33]:

$$H = H_0 + J_c \sum_i \mathbf{S}(R_i) \cdot \mathbf{J}(R_i), \tag{4.1}$$

where H_0 is a 16x16 matrix including both electronic dispersion and spin-orbit coupling of the sp^3 holes of the parent material. Our tight-binding parameters reproduce the correct band structure for the heavy and light bands around the center of the Brillouin zone, the split-off energy gap and the gap between the valence and the conduction bands[94, 95]. The spin-orbit coupling is modeled with a term $\lambda_\alpha \mathbf{L} \cdot \mathbf{S}$ where λ_{Ga} and λ_{As} are interaction constants for Ga and As atoms respectively. The second term in Eq. (5.1) describes the interaction between Mn spins and mediating holes, where J_c is the exchange coupling between the localized moments with spin $\mathbf{S}(R_i)$ and the total angular momentum density of holes $\mathbf{J}(R_i)$, both at site i. Since the spins of Mn^{2+}'s are relatively large ($S = 5/2$) we treat them as classical vectors.

We employ the DMFA algorithm [73] to calculate the magnetic and transport properties of the material within a Green's function formalism [47, 48]. Using the effective action (S_{eff}) we calculate the average magnetization of the manganese ions:

$$M = \frac{1}{\mathcal{Z}} \int d\Omega_s S^z \exp\{-S_{eff}(\mathbf{S})\} \tag{4.2}$$

with the partition function $\mathcal{Z} = \int d\Omega_s \exp[-\mathrm{S}_{\mathrm{eff}}(\mathbf{S})]$.

The average polarization of the charge carriers at the chemical potential is defined as:

$$\mathcal{P} = \frac{\sum_i j_i^z n_i(\mu)}{\sum_i n_i(\mu)} \tag{4.3}$$

with j_i^z the z component of the total angular momentum and n_i the density of the holes in the ith band.

To compute the optical conductivity we calculate the spectral function in real frequency and use the Kubo formula[97]:

$$\sigma_{ij}(\omega) = \frac{-1}{\omega} \int d\nu (f(\nu) - f(\omega + \nu)) \times \sum_k Tr(v_i(k) A(k, \nu) v_j(k) A(k, \omega + \nu)) \tag{4.4}$$

Tr is the trace of the matrix and $v_i(\mathbf{k})$ is the velocity in i direction. $A(\mathbf{k}, \omega)$ is the spectral function at momentum $\mathbf{k}$ and frequency (ω) and $f(\omega)$ is the Fermi function. Notice that both spectral functions have the same momentum index. This is because within the DMFA the momentum dependency of the self energy is ignored which leads to cancellation of the vertex contributions in the current-current correlation function $(\langle \mathbf{j}_i \mathbf{j}_j \rangle)$.

4.3 Results and Discussion

We first focus on the density of states (DOS) of the charge carriers at the doping x=0.05 where T_c is among the highest reported.[11, 26, 46] In Fig. 5.1 and 4.2 we assume 50% compensation for the mediating holes due to anti-site and interstitial doping, such that $\mathrm{n_h} = x/2 = 0.025$. This corresponds to optimum filling in the impurity band regime of the DMS. Fig. 5.1 shows the total density of states at the edge of the valence band for several values of coupling. Most experimental probes, such as photoemission [80], infrared [81, 98, 82], resonant tunneling [83] spectroscopy and magneto-transport experiments [84] infer a value of J_c between 0.6-1.5 eV. Within this range of couplings the effect of the magnetic interactions is just the distortion of the edge of the valence band. We have to use coupling strengths as large as 2.5 eV to be able to observe the formation of the impurity band. Fig. 5.1 shows the impurity band is not completely separated until very large couplings ($\sim 4eV$). However, we find that our result for large couplings ($J_c \sim 3.0eV$) is in agreement with recent experiments mapping the impurity band with the scanning tunneling microscopy.[99] The profile of the DOS changes minimally with filling. As we expected the repulsion between the conduction and the impurity band confines the latter within the band gap and narrows down the impurity bandwidth. This

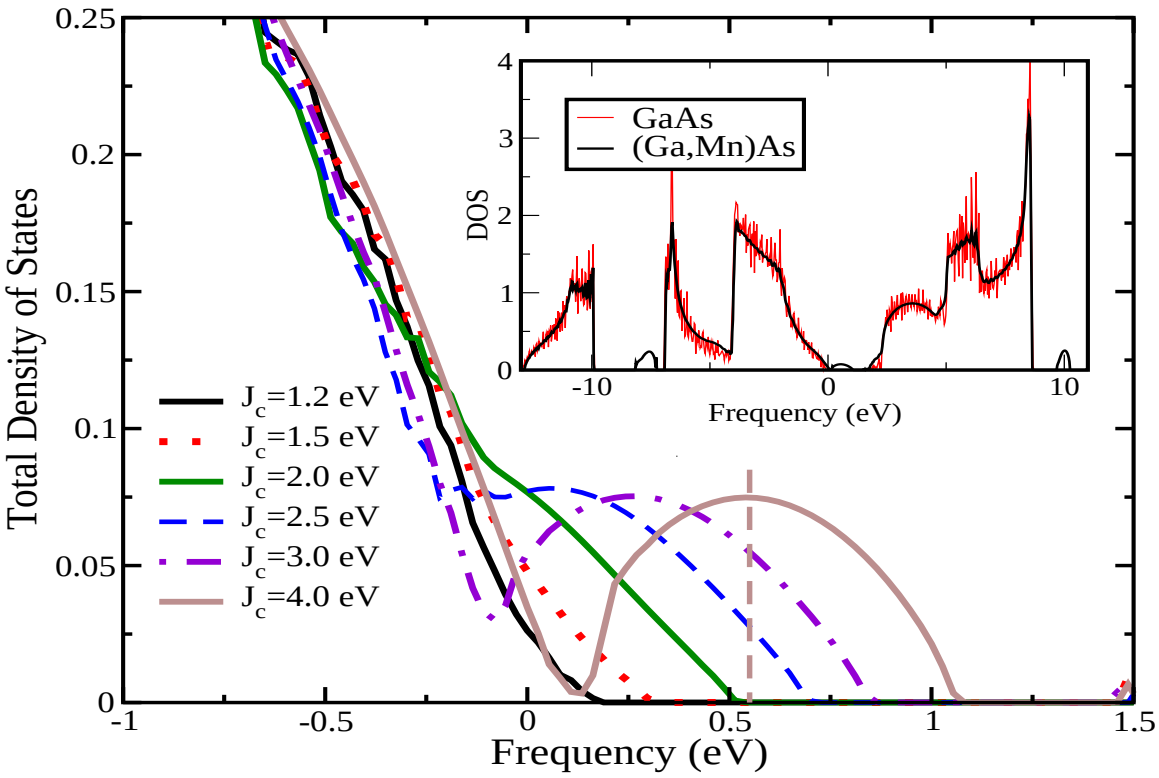

Figure 4.1: Total density of states versus energy at the edge of the valence band for $x = 0.05$, $n_h = x/2 = 0.025$ and several coupling strengths. The edge of the conduction band lies at the right bottom corner. The impurity band is not well separated from the valence band up to large couplings (J_c ∼4eV). The vertical dashed line shows the location of the chemical potential for J_c=4.0 eV. Band repulsion between the conduction and impurity bands leads to reduction of the impurity bandwidth. Inset: sp^3 total density of states for pure GaAs and $Ga_{0.95}Mn_{0.05}As$ with J_c=4.0 eV.

leads to localization of the charge carriers which in return reduces the ferromagnetic transition temperature, T_c, of the DMS. We use a Fourier transform filter to reduce the noise in the calculated density of states. The noise is in regions away from the Fermi energy and is due to the effect of the **k** mesh in the coarse graining step of the DMFA self-consistency loop. We have used up to 62000 **k** points in this calculation.

Fig. 4.2 displays the temperature dependence of the hole polarization for different couplings. It is evident from the figure that the average hole polarization is frustrated by decreasing of the coupling strength at T=0. We choose a narrow energy window (∼0.1 eV) at the chemical potential and calculated the average of $\mathcal{P}$ within this window. Comparison with Fig.5.1 shows that noticeable changes in T_c correspond to changes coupling regime where the impurity band is forming (separating) from the valence band and have minimum effect on T_c in the impurity band regime. It shows that the maximum T_c is ∼220K which is closer to experimental results (∼150K)[3] than previous simpler models.[47, 48] One can also see the same behavior from the inset which shows the changes in average magnetization of magnetic ions Mn^{2+} versus temperature.

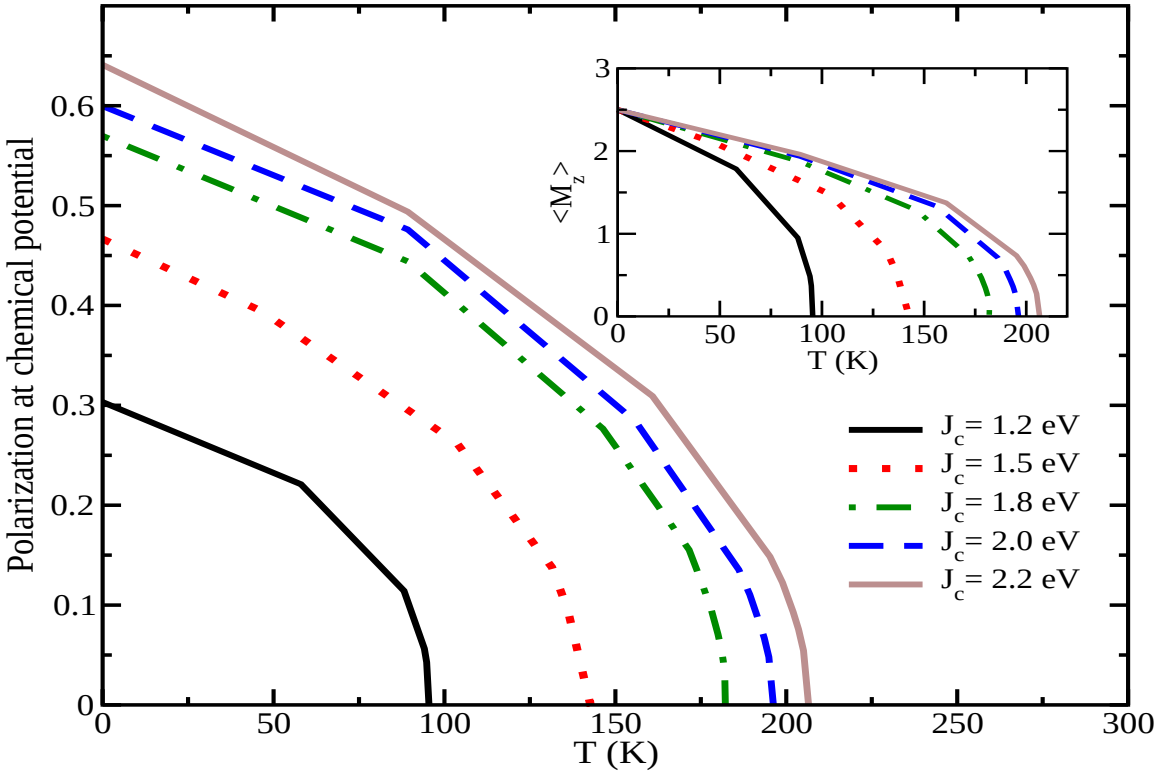

Figure 4.2: Average polarization of the holes vs. temperature for different values of J_c at $n_h = x/2 = 0.025$. The polarization is frustrated since it does not reach its maximum allowed value at $T = 0$. Comparison with Fig. 5.1 shows that noticeable changes in T_c happens when the impurity band is forming. Inset: Average magnetization of the ions versus temperature for the same couplings.

Figure 4.3 is the plot of T_c versus filling of the holes for different couplings. It shows ceiling for the IB regime, large J_c, at the optimum hole concentration ($n_f = x/2$). This is consistent with previous theories based on the impurity band picture.[47, 49] For the moderate regime of couplings (J_c ~1.5 eV) the figure shows that T_c increases by decreasing of the hole concentration larger than $n_f > 2\%$. While our model is for bulk, recent studies, based on deformation of the valence band, show in the thin films, the T_c is proportional to hole concentration for wide range of n_f [100, 101, 102]. Inset is the plot of T_c versus J_c for the fixed hole concentration ($n_f = x/2 = 2.5\%$). The plateau in at the large coupling values is due to absence of non-local correlations within the DMFA.

Finally we calculated the optical conductivity using (4.4). Figure 4.4 is the plot of σ_{xx} versus energy for different couplings. It shows photon energies up to the magnitude of the band gap. For smaller couplings, $J_c \leq 2.0eV$, the valence band is distorted, and conductivity shows the Drude like peak at low energy. The peak is suppressed upon increasing of coupling value. This is due to the fact that the bounding between magnetic ions and itinerant holes is stronger for larger couplings, and holes are more localized. Our result

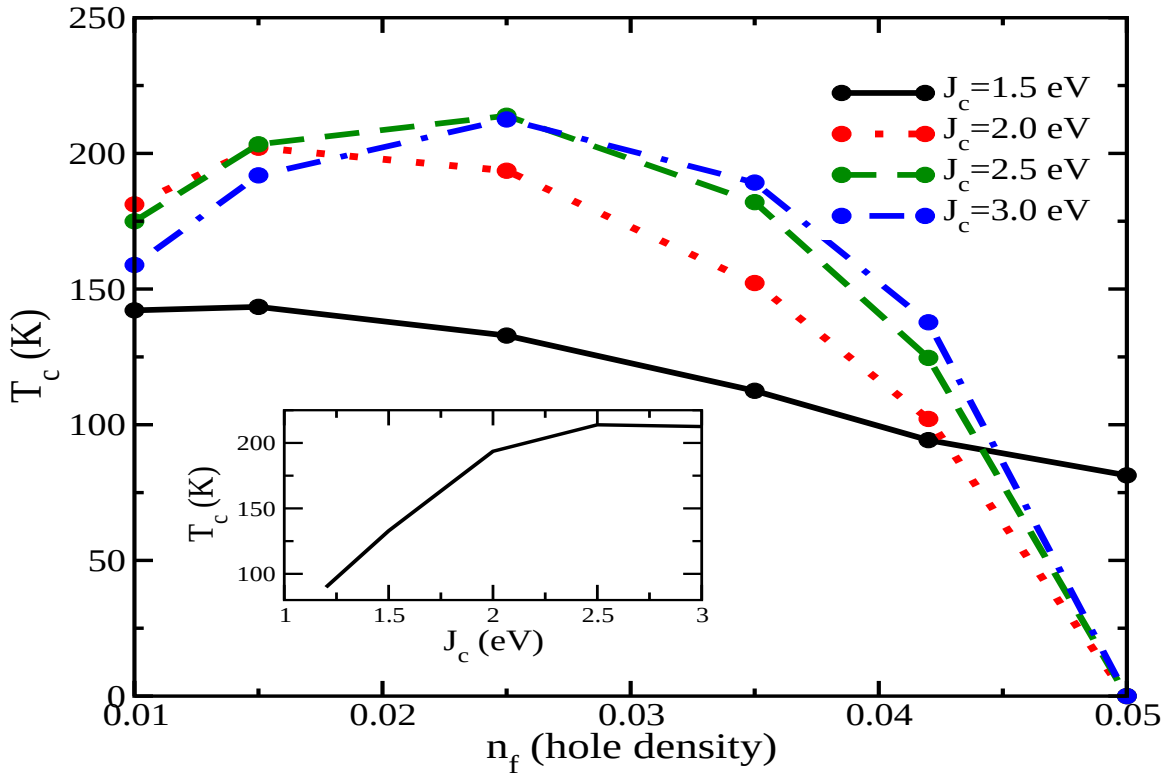

Figure 4.3: T_c versus filling for different couplings in constant doping (x=5%). For small couplings the T_c is suppressed by increasing It shows that the optimum filling for J_c greater for large couplings. This is consistent with Fig. 1 and 2 that for the coupling values lager than 2 eV, the changes in the magnetic properties of the DMS is less profound. Inset shows the saturation of the T_c with coupling strength at $n_f = x/2$. This is due to the lack of non-local correlations in the DMFA

is in agreement with other theoretical calculations[91], however, we could not capture the low energy (∼0.2 eV) peak in conductivity observed in experiment[103]. This is because, for smaller couplings the impurity band is not formed, and for large couplings, the wide impurity band suppresses all low energy features. The source of the peak is still the matter of controversy, while Burch *et al.* explain it as the evidence of the existence of the impurity band[103] others explain the result within the distorted valence band picture.[101]

4.4 Conclusions

We find more realistic band structure leads to more realistic results. In this paper we employ semi-empirical sp^3 tight binding approximation to model the band structure of the parent material (GaAs). We study the magnetic and transport properties of the diluted magnetic semiconductor $Ga_{1-x}Mn_xAs$ within the framework of the multi-orbital DMFA. We choose the tight binding parameters for the model according to Chadi

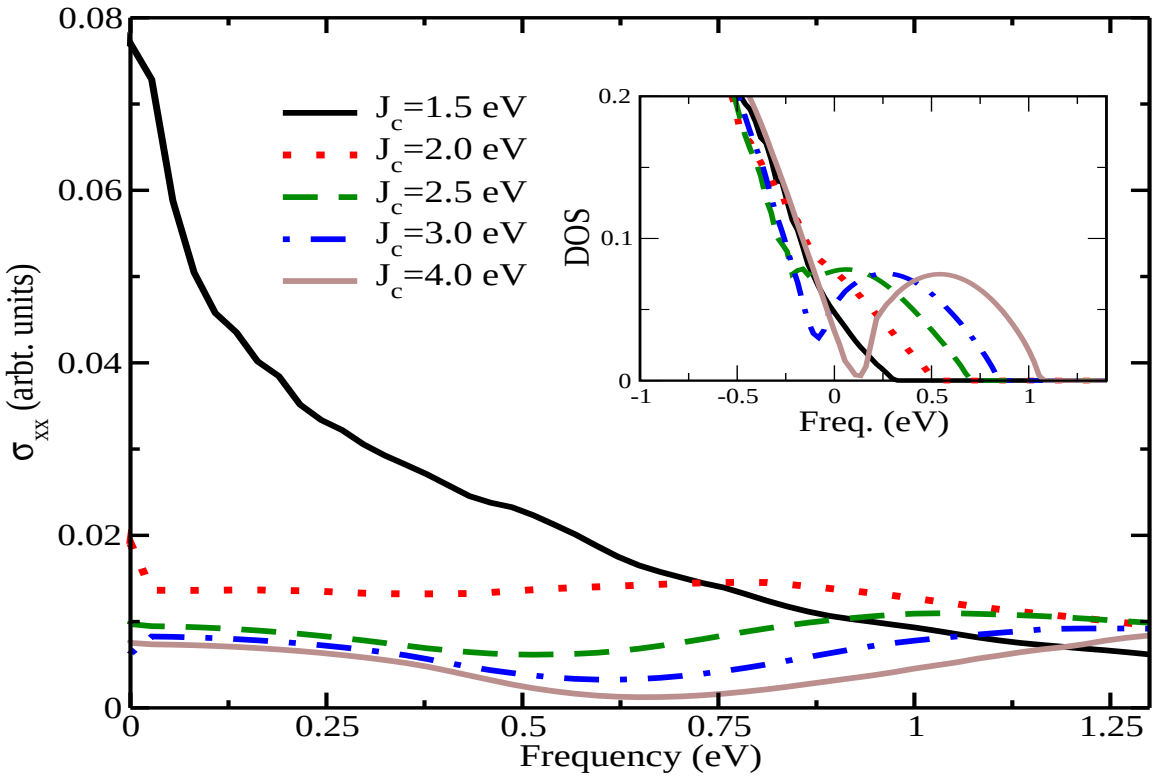

Figure 4.4: Optical conductivity in direction perpendicular to the magnetization in low temperatures for different couplings at n_f=2.5%. Conductivity is suppressed by increasing of J_c due to increase of the bonding of the holes to the magnetic ions.

[77], which give the correct band structure within the relevant energy range ($\sim \epsilon_f \pm$ 2.0 eV). This includes the valence, split-off and conduction bands (band gap). The calculated density of state shows the distorted valence instead of the impurity band for moderate regime of coupling strengths (J_c ~1.5 eV) and we have to apply large couplings (J_c ~3.0 eV) in order to observe the impurity band. The band repulsion between the impurity and conduction bands reduces the bandwidth of the impurity band for large couplings. This in turn leads to localization of the itinerant holes and reduction of the calculated T_c.

The average hole polarization ($\mathcal{P}$) of the holes is calculated from (5.3). The results show that the hole polarization is frustrated by decreasing of the coupling.

Moreover, calculated optical conductivity σ_{xx} shows the Drude like peak at low frequencies which is frustrated by increasing of the coupling. While our result is consistent with previous TB calculations, we could not capture the low energy peak (~0.2 eV) in the conductivity which was observed in experiment. Our explanation is that even with the inclusion of the conduction band, resulting in narrowing down the impurity bandwidth due to repulsion, the calculated impurity bandwidth is still too large (~1 eV). The wide impurity

band smears out the low energy features. We believe that the inclusion of corrections including cavity field and non-local correlations into the the mean field approximation result in further suppression of the impurity band width and possibly appearance of the peak in the conductivity.

Chapter 5

Magnetism in $Ga_{1-x}Mn_xN$

5.1 Introduction

The prediction of a ferromagnetic transition temperature well above room temperature for large band gap semiconductors in the pioneering work of Dietl *et al.* [67] has triggered a worldwide search for such material. Amongst wide band gap semiconductors, group III-nitrides (GaN, InN, AlN) are which have been in the center of much attention due to their intensive use in electronic devices[104, 105]. Perhaps one of the most studied DMS in this group is $Ga_{1-x}Mn_xN$, with a 3.39 eV gap at 300K for the parent compound[106]. GaN has stable wurtzite and metastable zinc-blende crystal structures. In this dissertation we focus on the stable wurtzite structure. According to theoretical predictions, based on static mean-field, $Ga_{1-x}Mn_xN$ might have one of the highest ferromagnetic transition temperatures well above room temperature[67]. However, reported T_c in $Ga_{1-x}Mn_xN$ varies from less that 2K [107] up to 940K [108]. This ambiguity in the transition temperature in (Ga,Mn)N, which is much more significant than in ($Ga_{1-x}Mn_xAs$, is due to the higher level of complexity in this material. Substitutional manganese ions can have two form in (Ga,Mn)N; Mn^{2+} with the d level deep into the valence band, just as (Ga,Mn)As, and Mn^{3+} whit d orbitals deep in the band gap[37, 38, 39, 107]. In the case of Mn^{2+} it is believed that the d orbitals are localized[20] but the real role of the mid gap d orbitals is still unknown[20, 36, 37]. Another issue is the small solubility of Mn in GaN, even smaller that GaAs,[39]. Out of equilibrium growth techniques, such as molecular beam epitaxy (MBE), increase the Mn density up to 10%[107, 109, 39], but at the same time it can lead to larger percentage of defects in the DMS. As already mentioned, defects in general reduce the concentration of the mediating holes, as well as, the effective doping. Moreover, excess in nitrogen vacancies, as a result of high temperature growth, increases the electronic density to the limit that make the DMS n-type[39, 109]. One can increase the hole concentration and restore the p-type DMS by doping the system with holes[32, 37]. A further issue that needs additional exploration is the formation of magnetic clusters in $Ga_{1-x}Mn_xN$ during the growth process. Experimental studies suggest that MnN regions in the DMS are responsible for observing high a

T_c, while in samples grown by well controlled growth process, with no such clusters, the T_c is less than 2K[39, 107, 110].

This is a continuation of our previous study of the DMS, where we employ a tight-binding (TB) Hamiltonian and the Dynamical Mean-Field Approximation (DMFA)[111]. Here we focus on the large band gap $Ga_{1-x}Mn_xN$. Pure GaN has two crystal structure, the stable wurtzite and metastable zinc-blende, which is stabilized upon doping[112]. In this dissertation we investigate the magnetism of the DMS in the wurtzite phase. The sp^3 TB parameters for the wurtzite structure are chosen following Kobayashi *et al.*[113] and Shulz *et al.*[114]. In the wurtzite crystal the unit cell is made of two gallium and two nitride atoms and care should be taken in applying mean-field approach for such structure.

We also study the effect of anisotropy on the magnetic properties of $Ga_{1-x}Mn_xN$. In general anisotropy in the DMS depends on crystal effects, hole concentration, and temperature in a complicated manner[11]. In the case of $Ga_{1-x}Mn_xN$ the anisotropy is more significant due to the small spin-orbit interaction[77]. Our calculations show the existence of an easy-axis along the hexagonal-c axis in the wurtzite crystal structure.

5.2 Model

We employ the simplified double-exchange Hamiltonian proposed by Zaránd and Jankó for the magnetic interactions between the magnetic ions and the itinerant holes[33]:

$$H = H_0 + J_c \sum_i \vec{\mathbf{S}}(R_i) \cdot \vec{\mathbf{J}}(R_i), \tag{5.1}$$

H_0 is the non-interacting Hamiltonian for the parent compound which includes both electronic dispersion and spin-orbit coupling. As mentioned before, the unit cell in wurtzite contains four atoms (two Ga and two N) thus, within sp^3 tight-binding, H_0 is a 32x32 matrix. We intorduce the spin-orbit interaction into our model with a simple form; $\lambda_{Ga}\vec{L} \cdot \vec{S}$ where $\vec{L}$ and $\vec{S}$ are angular momentum and spin of the charge carriers respectively. λ_{Ga} is the interaction constant at the gallium site. The spin-orbit effect is negligible at nitride site and we assume it is zero throughout our calculation. The second term is the magnetic interaction between the local magnetic moments ($\vec{\mathrm{S}}$) and itinerant holes with total angular momentum ($\vec{\mathrm{J}}$) at the impurity site (R_i). J_c is the the effective ferromagnetic exchange coupling. Here we assume $\vec{\mathrm{S}}$ is a classical moment due to its relative large magnitude (S=5/2). In our calculations we also assume Mn ions are in the Mn^{2+} state with the d band deep into the valence band.

We follow Furukawas's effective action method[58, 59, 115] to calculate the magnetic properties of

$Ga_{1-x}Mn_xN$ within the framework of the dynamical mean-field approximation[73]. Using the effective action (S_{eff}) we calculate the average magnetization of the manganese ions:

$$M = \frac{1}{\mathcal{Z}} \int d\Omega_s S^z \exp\{-S_{eff}(\mathbf{S})\} \tag{5.2}$$

with the partition function $\mathcal{Z} = \int d\Omega_s \exp[-\mathrm{S_{eff}}(\mathbf{S})]$.

We explore the effect of spin-orbit interaction on the magnetic frustration in the DMS by studying the hole polarization. The average polarization of the charge carriers at the chemical potential is defined as:

$$\mathcal{P} = \frac{\sum_i j_i^z n_i(\mu)}{\sum_i n_i(\mu)} \tag{5.3}$$

where j_i^z is the z component of the total angular momentum and n_i is the density of the holes in the ith band.

5.3 Results and Discussion

We start with the density of states of the charge carriers in the DMS, where we assume the effective doping is 5%. We keep the effective doping fixed at 5% throughout our calculations. We also assume that the holes are highly compensated due to defects and we take $\mathrm{n_f}$=2.5%. It is shown bellow this value corresponds to the optimum band filling in the impurity band regime. Figure 5.1 displays the total density of states (DOS) of the holes at the edge of the valence band for several couplings. The strength of the exchange coupling in $Ga_{1-x}Mn_xN$ is even more ambiguous than for $Ga_{1-x}Mn_xAs$ and to the best of our knowledge there is not a conclusive experimental result that shows its value. However, it is believed that the interaction in $Ga_{1-x}Mn_xN$ is stronger, but it has a shorter range, than in $Ga_{1-x}Mn_xAs$[37, 67, 116]. From this Figure it is clear that the impurity band is formed and completely separated from the valence band for coupling as small as J_c=0.8 eV. Comparing this results with the results of the last chapter one finds that the impurity band is well formed for smaller couplings than for $Ga_{1-x}Mn_xAs$. This is due to the fact that in GaN the valence band is flatter, thus its energy is closer to the Fermi energy, around the center of the Brillouin zone. In other words, heavier holes in $Ga_{1-x}Mn_xN$ form the impurity band for smaller couplings. This is in agreement with our result of Chapter Two where introduction of the spin-orbit interaction in the DMS enhances the formation of the impurity band. It is also evident from this Fig. 5.1 that a small change in the coupling, from J_c=0.6 to 0.8 eV, has a significant change on the density of states of the charge carriers. We confirm that changes in the hole concentration have a small effect on the density of states. The large band gap in this

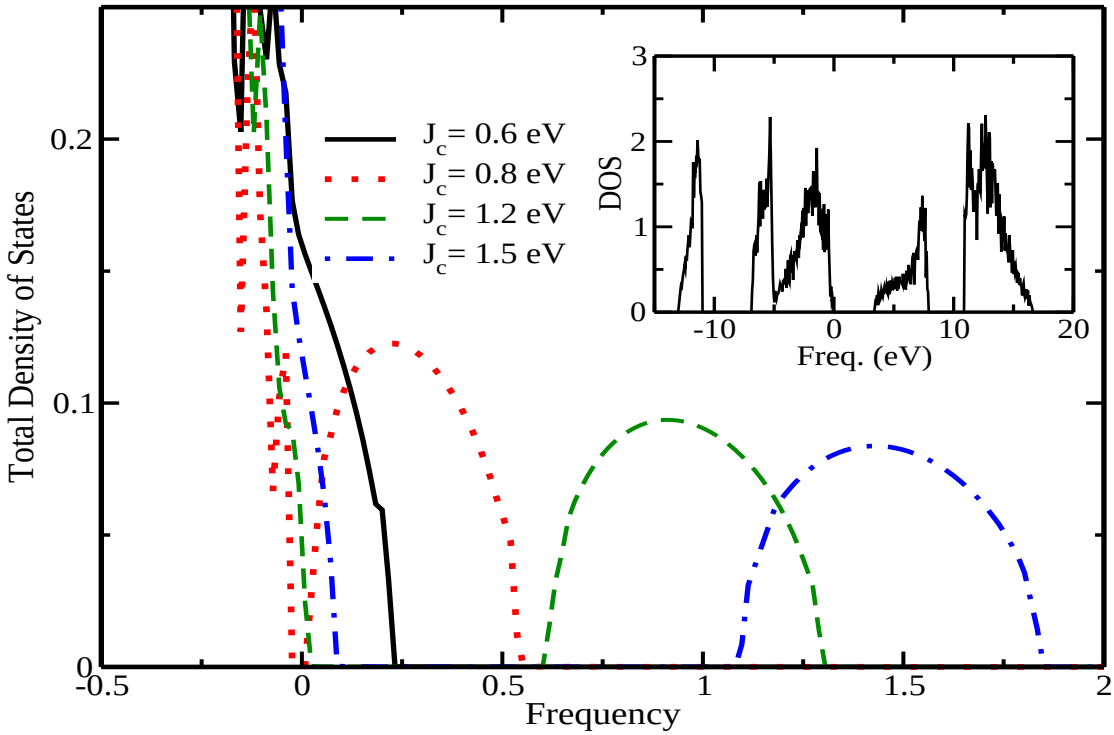

Figure 5.1: Total density of states versus energy at the edge of the valence band for $x = 0.05$, $n_h = x/2 = 0.025$, at T=46K. The impurity band is completely formed at J_c=0.8 eV. One can see drastic changes in the density of states by increasing the coupling from J_c=0.6 to 0.8 eV. Inset: sp^3 total density of states for pure GaN.

material reduces the effect of band repulsion between the impurity band and the conduction band. However, impurity bandwidth is comparable with the bandwidth in (Ga,Mn)As.

Figure 5.2 illustrates the dependency of the average hole polarization on the temperature for several coupling values at n_f=2.5%. It is evident that a change in the magnetic coupling has minimum effect on the ferromagnetic transition temperature at large couplings. This is in agreement with the results of previous chapters. The average hole polarization at T=0 is significantly larger than what we find for $Ga_{1-x}Mn_xAs$ in the last chapter. This is due to much smaller spin-orbit interaction in GaN, ∼17 meV, than in GaAs, ∼340 meV. The inset is the average magnetization of the magnetic impurity versus temperature for the same set of parameters.

Finally, Figure 5.3 illustrates the dependence of the T_c on hole concentration for different couplings. Compared with Figure 5.1, it is clear that there is a maximum in T_c when the coupling is large enough to form the impurity band. The maximum T_c corresponds to half filling in the impurity band regime. One can see that the maximum T_c in this material is ∼220K which is in clear contradiction to the studies based on

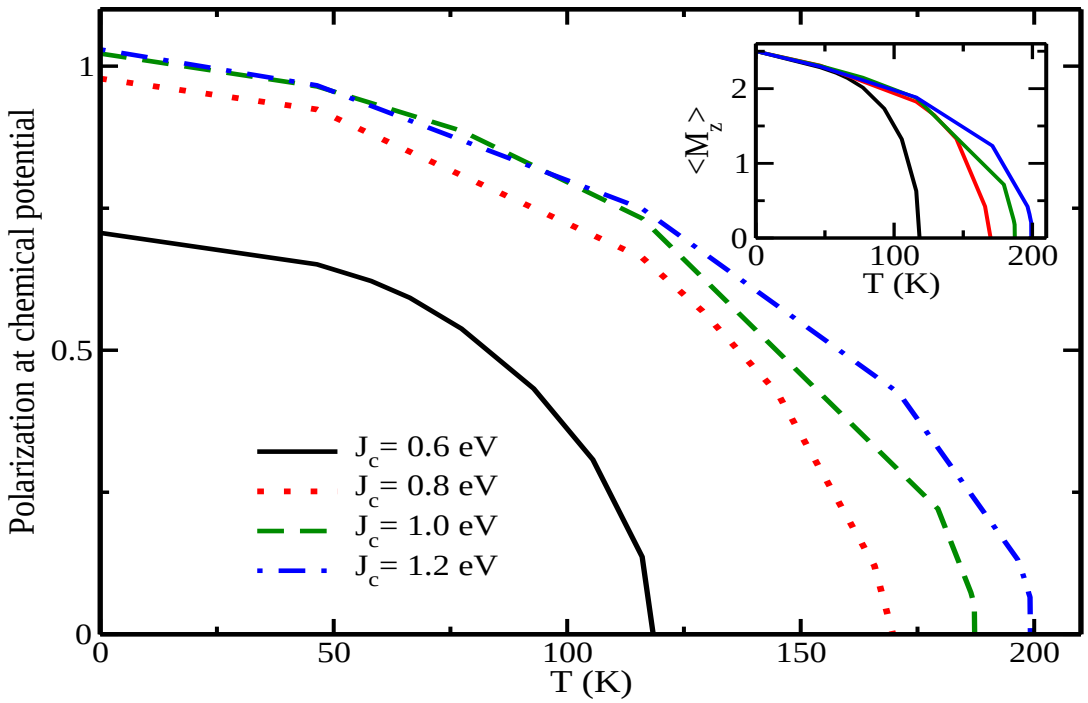

Figure 5.2: Average hole polarization vs. temperature for different magnetic couplings (J_c) at n_f=$x/2$=0.025. It is clear that changes in J_c have smaller effect on the ferromagnetic transition temperature in the large coupling regime. The magnetic frustration due to spin-orbit interaction is evident from the polarization at T=0. Inset is the average moment of the magnetic impurity vs. temperature

the static mean-field theory. Static mean-field calculations predict T_c well over room temperature for the wide gap DMS[67]. Our calculations show that the maximum T_c for $Ga_{1-x}Mn_xN$ is comparable with the results in the previous chapter, for $Ga_{1-x}Mn_xAs$,. We expect non-local correlations in this DMS suppress ferromagnetism.

5.4 Conclusions

We find that the wurtzite structure has an easy-axis along the hexagonal-c axis with a higher ferromagnetic transition temperature than for other directions. We explore ferromagnetism in $Ga_{1-x}Mn_xN$ in a wide range of magnetic couplings, from the distorted valence band, to well into the impurity band regimes. Our calculation show that the impurity band is formed for much smaller couplings in $Ga_{1-x}Mn_xN$ compared to $Ga_{1-x}Mn_xAs$. Despite of using large couplings our calculations show maximum T_c well below room temperature as opposed to the static mean-filed predictions. Take into consideration that the calculated

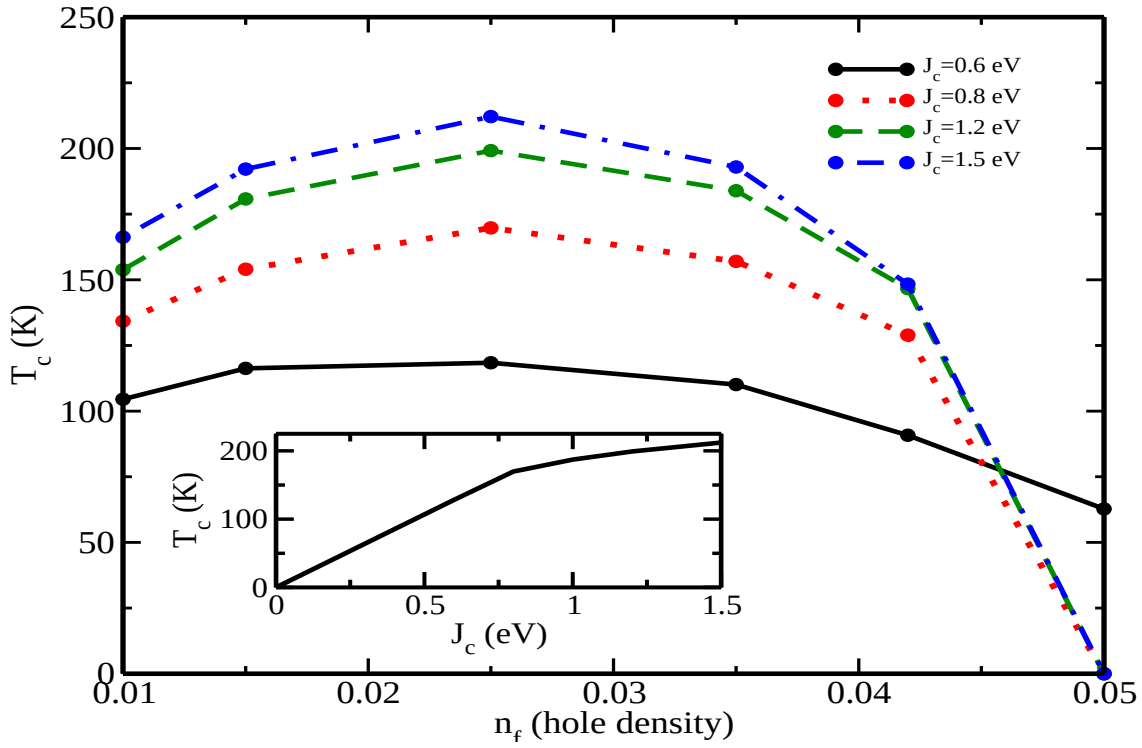

Figure 5.3: T_c vs. hole concentration for different couplings. The optimum filling of n_f=$x/2$=0.025, maximizes the T_c in the impurity band regime (compare with Fig. 5.1). Inset shows the saturation of the T_c with coupling strength at $n_f = x/2$. This is due to the lack of non-local correlations in the DMFA.

T_c within the DMFA is overestimated, due to the lack of non-local correlations, we expect such corrections suppress T_c even more. However, one has to go well beyond mean-field in order to reach T_c as low as 2K[107]. Based of our calculation, we predict the quenched $Ga_{1-x}Mn_xN$ with magnetic impurities in the Mn^{2+} state, has a T_c comparable with $Ga_{1-x}Mn_xAs$. We also notice that the magnetic frustration in $Ga_{1-x}Mn_xN$ is less profound compared with $Ga_{1-x}Mn_xAs$, due to the smaller spin-orbit interaction in the former.

Chapter 6

Summary

6.1 Summary

The magnetic and transport properties of the diluted magnetic semiconductors (DMS) has been studied. This dissertation focuses on $Ga_{1-x}Mn_xAs$ and wide band-gap $Ga_{1-x}Mn_xN$ as two important candidates for spintronic devices. We model the magnetic interaction in the DMS with the double-exchange interaction, where the magnetic interaction is mediated by itinerant charge carriers. We adopt a simplified form for the double-exchange which was proposed by Zaránd and Jankó. Doping the semiconductor with magnetic impurities is assumed to have a minimum effect on the band structure of the material, thus we employ the same dispersion for both parent compound and the DMS. We start with the two-band $k \cdot p$ model and improved our model by using the more sophisticated sp^3 tight-binding Hamiltonian for the dispersion of the parent material. We also incorporate non-local correlations into the DMS.

In Chapter 2, we investigate the effect of the attractive Coulomb attraction between the magnetic impurities and the itinerant holes on the ferromagnetism of $Ga_{1-x}Mn_xAs$. Our calculations show that the Coulomb potential enhances the ferromagnetism in the DMS. We also study the effect of the spin-orbit interaction (SO) on the DMS. We find that for the large $J_c - V$, the SO interaction suppresses T_c, while in the small parameters regime, ferromagnetism is enhanced by the SO interaction. We find that both the Coulomb and the spin-orbit interactions enhance the formation of the impurity band.

In Chapter 3, we introduce non-local correlations into the above-mentioned two-band model of the DMS by using the Dynamical Cluster Approximation (DCA) . We use several clusters and find that correlations between nearest neighbor impurities have biggest effect on the ferromagnetism in the DMS. Our calculations show that such correlations lead to configurational magnetic frustration and suppress the ferromagnetic transition temperature to the extent that our results are in good agreement with experimental results. We also study the effect of the strain on the ferromagnetism of the DMS. We show that the tensile strain leads to perpendicular-to-plane magnetization, while compressive strain alines the moment in the plane of growth.

Moreover, we are the first to show that non-local correlations between nearest neighbor impurities cause the temperature dependent rotation of the in-plane magnetic moment, a phenomenon that has been observed in experiments.

In Chapter 4, we improve our DMFA model by using a more realistic band structure for the parent compound in $Ga_{1-x}Mn_xAs$. We employ the sp^3 tight-binding (TB) Hamiltonian with more realistic features within the relevant energy scale. Especially important is the effect of inclusion of the conduction band on the properties of the DMS. We find that the more realistic band structure leads to more realistic results. We find that the overestimated T_c in the second Chapter is suppressed upon using the sp^3 TB Hamiltonian. Incorporation of the conduction band into the model results in decrease of the impurity bandwidth and thus localization of the mediating holes. We also study the effect of the spin-orbit interaction on the averaged hole polarization. We find that the the SO interaction significantly suppresses the hole polarization. Finally, we study the optical conductivity of the DMS. Although our results are in agreement with other theoretical studies we could not capture the low energy peak in the conductivity. We conclude that non-local correlations are needed to narrow down the impurity bandwidth and capture the low energy peak in the conductivity.

In Chapter 5, we study the wide band gap $Ga_{1-x}Mn_xN$. We employ the sp^3 tight-binding Hamiltonian for the more complicated wurtzite structure with four atoms in the unit cell. Based on a simple argument relating the coupling constant with the inverse of the lattice constant, static mean-field calculations predict a large ferromagnetic transition temperature for this material. However, our DMFA calculations show that the T_c is comparable with the one of $Ga_{1-x}Mn_xAs$ and significantly smaller than room temperature. We also find that the impurity bandwidth in the $Ga_{1-x}Mn_xN$ is comparable to the one in $Ga_{1-x}Mn_xAs$, despite the smaller effect of the conduction band in this large band gap material. Moreover, the average hole polarization is larger in $Ga_{1-x}Mn_xN$ due to the weaker spin-orbit interaction in this material.

6.2 Future Directions

In this dissertation, the DMFA and the DCA techniques have been used for the simplified two-band $k \cdot p$ model of the DMS. Within the DMFA, we were able to capture the qualitative behavior of the DMS. Incorporation of the spatial correlations to the model, through the DCA, has led to more realistic results for the ferromagnetic transition temperature. Moreover, we were able to explain the temperature dependent reorientation of the magnetic moment in the DMS, which is a highly non-local effect. However, there is some inaccuracy in some of the results of the two-band model. For example, our prediction of the impurity bandwidth in not accurate. We use a more realistic sp^3 tight-binding (TB) Hamiltonian to fix some of the

shortcomings of the two-band model. The sp^3 tight-binding Hamiltonian incorporates the conduction band into the band structure of the DMS, and the resulting impurity bandwidth is smaller than the two-band prediction. Nevertheless, our DMFA study overestimates the impurity bandwidth. A natural improvement to the model is incorporating non-local interactions, via the DCA or other corrections such as the cavity field. We expect that the combined effects of the conduction band and spatial correlations further decrease the width of the impurity band.

It would also be interesting to study the effect of strain on the magnetism of the DMS. This is because the best DMS, with high T_c, are grown by epitaxial techniques, where strain is due to the lattice constant mismatch between the sample and the substrate. In multi-orbital models however, strain has a rather complicated form, and might lead to non-trivial results.

In our study, we ignore the attractive potential amongst magnetic impurities. However, in out of equilibrium growth, the attractive potential is essential for the formation of magnetic clusters. A very interesting study, would be to explore the effect of magnetic clusters on the properties of the DMS. Especially important, is this effect in the heterostructure DMS, since it leads to the formation of micro-columns of magnetic impurities. It is believed that these micro-columns are responsible for a high T_c in the heterostructure DMS.

References

[1] B. S. Sørensen, P. E. Lindelof, J. Sadowski, R. Mathieu, and P. Svedlindh, "Effect of annealing on carrier density and Curie temperature in epitaxial (Ga,Mn)As thin films," *Appl. Phys. Lett.*, vol. 82, p. 2287, 2003.

[2] C. K.Ku, J. Potashnik, R. F. Wang, S. H. Chun, P. Schiffer, N. Samarth, M. J. Mascarenhas, E. Johnston-Halperin, R. C.Myers, A. C. Gossard, and D. D. Awshalom, "Highly enhanced Curie temperature in low-temperature anneald [Ga,Mn]As epilayers," *Appl. Phys. Lett.*, vol. 82, p. 2302, 2003.

[3] K. Y. Wang, K. W. Edmonds, R. P. Campion, B. L. Gallagher, N. R. S. Farley, C. T. Foxon, M. Sawicki, P. Boguslawski, and T. Dietl, "Influence of the Mn interstitial on the magnetic and transport properties of (Ga,Mn)As," *J. Appl. Phys*, vol. 95, p. 6512, 2004.

[4] M. Sawicki, F. Matsukura, A. Idziaszek, T. Dietl, G. M. Schott, C. Ruester, C. Gould, G. Karczewski, G. Schmidt, and L. W. Molenkamp, "Temperature dependent magnetic anisotropy in (Ga,Mn)As layers," *Phys. Rev. B*, vol. 70, p. 245325, 2004.

[5] K. Y. Wang, M. Sawicki, K. W. Edmonds, R. P. Campion, S. Maat, C. T. Foxon, B. L. Gallagher, and T. Dietl, "Spin Reorientation Transition in Single-Domain (Ga,Mn)As," *Phys. Rev. Lett.*, vol. 95, p. 217204, 2005.

[6] U. Welp, V. K. Vlasko-Vlasov, X. Liu, J. K. Furdyna, and T. Wojtowicz, "Magnetic Domain Structure and Magnetic Anisotropy in $Ga_{1-x}Mn_xAs$," *Phys. Rev. Lett.*, vol. 90, p. 167206, 2003.

[7] S. C. Masmanidis, H. X. Tang, E. B. Myers, M. Li, K. D. Greve, G. Vermeulen, W. V. Roy, and M. L. Roukes, "Nanomechanical Measurement of Magnetostriction and Magnetic Anisotropy in (Ga,Mn)As," *Phys. Rev. Lett.*, vol. 95, p. 187206, 2005.

[8] N. F. Mott and R. Reierls, "," *Proc. Phys. Soc. London A*, vol. 49, p. 72, 1937.

[9] J. Kondo, "Resistance Minimum in Dilute Magnetic Alloys," *Prog. Theor. Phys.*, vol. 32, p. 37, 1964.

[10] P. W. Anderson and H. Hasegawa, "Localized Magnetic States in Metals," *Phys. Rev.*, vol. 124, p. 41, 1961.

[11] H. Ohno, "Making Nonmagnetic Semiconductors Ferromagnetic," *Science*, vol. 281, p. 951, 1998.

[12] H. Ohno, "Properties of ferromagnetic III-V semiconductors," *J. of Mag. and Mag. Mat.*, vol. 200, pp. 110–129, 1999.

[13] F. Matsukura, H. Ohno, A. Shen, and Y. Sugawara, "Transport properties and origin of ferromagnetism in (Ga,Mn)As," *Phys. Rev. B*, vol. 57, pp. R2037–R2040, 1998.

[14] I. Zutic, J. Fabian, and S. D. Sarma, "Spintronics: Fundamentals and applications," *Rev. Mod. Phys.*, vol. 76, pp. 323–410, 2004.

[15] S. A. Wolf, D. D. Awshalom, R. A. Buhrman, J. M. Daughton, S. von Molnar, M. L. Roukes, A. Y. Chtchelkanova, and D. M. Treger, "Spintronics: A Spin-Based Electronics Vision for the Future," *Science*, vol. 94, p. 1488, 2001.

[16] Y. Ohno, D. K. Young, B. Beschoten, F. Matsukura, H. Ohno, and D. D. Awshalom, "Electrical spin injection in a ferromagnetic semiconductor heterostructure," *Nature*, vol. 402, p. 790, 1999.

[17] A. M. Nazmul, T. Amemiya, Y. Shuto, S. Sugahara, and M. Tanaka, "High Temperature Ferromagnetism in GaAs-Based Heterostructures with Mn δ Doping," *Physical Review Letters*, vol. 95, pp. 017201/1–4, June 2005.

[18] A. H. MacDonald, P. Schiffer, and N. Samarth, "Ferromagnetic semiconductors: moving beyond (Ga,Mn)As," *Nature Materials*, vol. 4, p. 195, 2005.

[19] M. L. Reed, N. A. El-Masry, H. H. Stadelmaier, M. K. Ritum, and M. J. Reed, "Room temperature ferromagnetic properties of (Ga,Mn)N," *Applied Physics Letters*, vol. 79, p. 3473, 2001.

[20] T. Jungwirth, J. Sinova, J. Mašek, J. Kučera, and A. H. MacDonald, "Theory of ferromagnetic (III,Mn)V semiconductors," *Reviews of Modern Physics*, vol. 78, pp. 809–864, July 2006.

[21] J. Blinowski and P. Kacman, "Spin intraction of interstitial Mn ions in ferromagnetic GaMnAs," *Phys. Rev. B*, vol. 67, p. 121204(R), 2003.

[22] J. Mašek and F. Máca, "Interstitial Mn in (Ga,Mn)As: Binding energy and exchange coupling," *Phys. Rev B*, vol. 69, p. 165212, 2004.

[23] F. Máca and J. Mašek, "Electronic states in $Ga_{1-x}Mn_xAs$: Sebstitutional versus interstitial of Mn," *Phys. Rev. B*, vol. 65, p. 235209, 2002.

[24] K. W. Edmonds, , K. Y. Wang, R. P. Campion, A. S. Neuwmann, N. R. S. Farley, B. L. Gallagher, and C. T. Foxon, "High-Curie-temperatureMn $Ga_{1-x}Mn_xAs$ obtained by resistance-monitored annealing," *Phys. Rev. Lett.*, vol. 81, p. 4991, 2002.

[25] K. M. Yu, W. Walukiewicz, T. Wojtowicz, I. Kuryliszyn, X. Liu, Y. Sasaki, and J. K. Furdyna, "Effect of the location of Mn sites in ferromagnetic $Ga_{1-x}Mn_xAs$ on its Curie temperature," *Phys. Rev. B*, vol. 65, p. 201303(R), 2002.

[26] D. Chiba, K. Takamura, F. Matsukura, and H. Ohno, "Effect of low-temperature annealing on (Ga,Mn)As trilayer structure," *Appl. Phys. Lett.*, vol. 82, p. 3020, 2003.

[27] H. Ohno, A. Shen, F. Matsukura, A. Oiwa, A. Endo, S. Katsumoto, and Y. Iye, "(ga,mn)as: A new diluted magnetic semiconductor based on gaas," *Appl. Phys. Lett.*, vol. 69, p. 363, 1996.

[28] J. M. D. Coey, M. Viret, and S. von Molnar, "Mixed-valence manganites," *Advances in Physics*, vol. 48, pp. 167–293, 1999.

[29] H. Akai, "Ferromagnetism and Its Stability in the Diluted Magnetic Semiconductor (In,Mn)As," *Phys. Rev. Lett.*, vol. 81, p. 3002, 1998.

[30] C. Zener, "Interaction between the d-Shells in the Transition Metals. II. Ferromagnetic Compounds of Manganese with Perovskite Structure," *Phys. Rev.*, vol. 82, pp. 403–405, 1951.

[31] T. Dietl *in Handbook of Semiconductors, editel by S. Mahajan (North-Holland, Amsterdam)*, vol. 3B, p. 1251, 1994.

[32] L.-F. Zhu and B.-G. Liu, "Curie temperature of cubic (Ga,Mn)N diluted magnetic semiconductors from the RKKY spin model," *J. Physs. Condens. Matter*, vol. 21, p. 446005, 2009.

[33] G. Zaránd and B. Jankó, "$Ga_{1-x}Mn_xAs$: A Frustrated Ferromagnet," *Phys. Rev. Lett.*, vol. 89, pp. 047201/1–4, 2002.

[34] J. M. Luttinger and W. Kohn, "Motion of electrons and holes in perturbed periodic fields," *Phys. Rev.*, vol. 97, pp. 869–883, Feb 1955.

[35] T. Dietl, "Hole states in widr band-gap diluted magnetic semiconductors and oxides," *Phys. Rev. B*, vol. 77, p. 085208, 2008.

[36] P. Mahadevan and S. Mahalakshmi, "Suitability of p-type conditions foro ferromagnetism in GaN:Mn," *Phys. Rev. B*, vol. 73, p. 153201, 2006.

[37] T. Schulthess, W. M. Temmerman, Z. Szotek, W. H. Butler, and G. M. Stocks, "Electronic structure and exchange coupling on Mn impurities in III-V semiconductors," *Nature Material*, vol. 4, p. 383, 2005.

[38] E. Sarigiannidou, F. Wilhelm, E. Monroy, R. M. Galera, E. Bellet-Amalric, A. Rogalev, J. Goulon, J. Cibert, and H. Mariette, "Intronsic ferromagnetism in wurtzite (Ga,Mn)As semiconductor," *Phys. Rev. B*, vol. 74, p. 041306R, 2006.

[39] T. Graf, M. Gjukic, M. S. Brandt, and M. Stutzmann, "The $Mn^{3+/2+}$ acceptor level in group III nitrides," *Appl. Phys. Lett.*, vol. 81, p. 5159, 2002.

[40] M. Jarrell, "The Hubbard Model in Infinite Dimensions: A Quantum Monte Carlo Study," *Phys. Rev. Lett.*, vol. 69, pp. 168–171, 1992.

[41] A. Georges and G. Kotliar, "Hubbard model in infinite dimensions," *Phys. Rev. B*, vol. 45, pp. 6479–6482, 1992.

[42] E. Müller-Hartmann, "Correlated fermions on a lattice in high dimensions," *Z. Phys. B (Condensed Matter)*, vol. 74, pp. 507–512, 1989.

[43] W. Metzner and D. Vollhardt, "Correlated lattice fermions in $d = \infty$ dimensions," *Phys. Rev. Lett.*, vol. 62, pp. 324–327, 1989.

[44] M. Hettler, M. Mukherjee, M. Jarrell, and H. Krishnamurthy, "The Dynamical Cluster Approximation: Nonlocal Dynamics of Correlated Electron Systems," *Phys. Rev. B*, vol. 61, pp. 12739–12756, 2000.

[45] M. R. P. K. Baltzer, P. J. Wojtowicz and E. Lopatin, "Exchange Interactions in Ferromagnetic Chromium Chalcogenide Spinels," *Phys. Rev.*, vol. 151, pp. 367,1–11, 1966.

[46] H. Munekata, H. Ohno, S. von Molnar, A. Segmüller, L. Chang, and L. Esaki, "Diluted magnetic III-V semiconductors," *Phys. Rev Lett.*, vol. 63, pp. 1849–1852, 1989.

[47] K. Aryanpour, J. Moreno, M. Jarrell, and R. Fishman, "Magnetism in semiconductors: A dynamical mean field study of ferromagnetism in $Ga_{1-x}Mn_xAs$," *Phys. Rev. B*, vol. 72, pp. 045343/1–6, 2005.

[48] M. Majidi, J. Moreno, M. Jarrell, R. Fishman, and K. Aryanpour, "Dynamics of Impurity and Valence Bands in GaMnAs within the Dynamical Mean Field Approximation," *Phys. Rev. B.*, vol. 74, pp. 115205/1–5, 2006.

[49] J. Moreno, R. S. Fishman, and M. Jarrell, "Transition Temperature of a Magnetic Semiconductor with Angular Momentum j," *Phys. Rev. Lett.*, vol. 96, pp. 237204/1–4, 2006.

[50] M. Takahashi and K. Kubo, "Carrier states and ferromagnetism in diluted magnetic semiconductors," *J. Phys. Soc. Jpn*, vol. 72, pp. 2866/1–14, 2003.

[51] F. Popescu, C. Sen, E. Dagotto, and A. Moreo, "Crossover from impurity to valence band in diluted magnetic semiconductors: Role of coulomb attraction by acceptors," *Phys. Rev. B*, vol. 76, pp. 85206/1–8, 2007.

[52] M. J. Calderón, G. Gómez-Santoz, and L. Brey, "Impurity-semiconductor band hybridization effects on the critical temperature of diluted magnetic semiconductors," *Phys. Rev. B*, vol. 66, p. 075218, 2002.

[53] E. H. Hwang and S. D. Sarma, "Transport properties of diluted magnetic semiconductors: Dynamical mean-field theory and Boltzmann theory," *Phys. Rev. B.*, vol. 72, p. 35210, 2005.

[54] A. Moreo, Y. Yildrim, and G. Alvarez, "Multi-Orbital Lattice Model for (Ga,Mn)As and other Lightly Magnetically Doped Zinc-Blende-Type Semiconductors," *cond-mat/0710.0577*, 2007.

[55] D. Taylor, "Vibrational Properties of Imperfect Crystals with Large Defect Concentrations," *Phys. Rev.*, vol. 156, pp. 1017–1029, 1967.

[56] P. Soven, "Coherent-Potential Model of Substitutional Disordered Alloys," *Phys. Rev.*, vol. 156, pp. 809–813, 1967.

[57] P. L. Leath and B. Goodman, "Displacement correlations and frequency spectra for mass-disordered lattices," *Phys. Rev.*, vol. 148, pp. 968–973, Aug 1966.

[58] N. Furukawa, "Thermodybamics of the Double Exchange Systems," *cond-mat/9812066*, pp. 1–35, 1998.

[59] N. Furukawa, "Transport Properties of Kondo Lattice Model in the Limit S=∞ and D=∞," *J. Phys. Soc. Jpn.*, vol. 63, pp. 3214/1–4, 1994.

[60] H. Ohno, D. Chiba, F. Matsukura, T. Omiya, E. Abe, T. Dietl, Y. Ohno, and K. Ohtani, "Electric-field control of ferromagnetism," *Nature*, vol. 408, p. 944, 2000.

[61] U. Yu, A.-M. Nili, K. Mikelsons, B. Moritz, J. Moreno, and M. Jarrell, "Non-local effects on magnetism in the diluted magnetic semiconductor $Ga_{1-x}Mn_xAs$," *Phys. Rev. Lett.*, vol. 104, p. 37201, 2010.

[62] P. Y. Yu and M. Cardona, *Fundamentals of Semiconductors*. Springer, 2001.

[63] in *spintronics* (T. Dietl, D. D. Awschalom, M. Kaminska, and H. Ohno, eds.), Academic Press, New York, 2008.

[64] P. Mahadevan, A. Zunger, and D. D. Sarma, "Unusual Directional Dependence of Exchange Energies in GaAs Diluted with Mn: Is the RKKY Description Relevant?," *Phys. Rev. Lett.*, vol. 93, p. 177201, 2004.

[65] J. Kudrnovský, , I. Turek, V. D. F. Máca, P. Weinberger, and P. Bruno, "Exchange interactions in V-III and group-V diluted semiconductors," *Phys. Rev B*, vol. 69, p. 115208, 2004.

[66] D. Kitchen, A. Richardella, J.-M. Tang, M. E. Flatté, and A. Yazdani, "Atom-by-atom substitution of Mn in GaAs and visualization of their hole-mediated interactions," *Nature*, vol. 442, p. 436, 2006.

[67] T. Dietl, H. Ohno, F. Matsukura, J. Cibert, and D. Ferrand, "Zener Model Desciption of Ferromagnetism in Zinc-Blend Magnetic Semiconductors," *Science*, vol. 287, pp. 1019–1022, 2000.

[68] J. D. J. Priour, E. H. Hwang, and S. D. Sarma, "Disordered RKKY Lattice Mean Field Theory for Ferromagnetism in Diluted Magnetic Semiconductors," *Phys. Rev. Lett.*, vol. 92, p. 117201, 2004.

[69] R. Bouzerar, G. Bouzerar, and T. Ziman, "Why RKKY exchange integrals are inappropriate to describe ferromagnetism in diluted magnetic semiconductors," *Phys. Rev. B*, vol. 73, p. 024411, 2006.

[70] A. Chattopadhyay, S. D. Sarma, and A. Millis, "Transition Temperature of Ferromagnetic Semiconductors: A Dynamical Mean Field Study," *Phys. Rev. Lett.*, vol. 87, pp. 227202/1–4, 2001.

[71] L. Craco, M. S. Laad, and E. Müller-Hartmann, "*Ab initio* description of the diluted magnetic semiconductor $Ga_{1-x}Mn_xAs$ Ferromagnetism, electronic structure, and optical response," *Phys. Rev. B*, vol. 68, p. 2333310, 2003.

[72] F. Popescu, Y. Yildirim, G. Alvarez, A. Moreo, and E. Dagotto, "Critical temperature of the two-band model for diluted magnetic semiconductors," *Phys. Rev. B*, vol. 73, p. 075206, 2006.

[73] A. Georges, G. Kotliar, W. Krauth, and M. Rozenberg, "Dynamical mean-field theory of strongly correlated fermion systems and the limit of infinite dimensions," *Rev. Mod. Phys.*, vol. 68, pp. 13–125, 1996.

[74] T. Maier, M. Jarrell, T. Pruschke, and M. Hettler, "Quantum Cluster Theories," *Reviews of Modern Physics*, vol. 77, pp. 1027–1080, 2005.

[75] M. Jarrell and H. Krishnamurthy, "Systematic and Causal Corrections to the Coherent Potential Approximation," *Phys. Rev. B*, vol. 63, pp. 125102/1–10, 2001.

[76] B. Moritz, K. Mikelsons, J. Moreno, R. Fishman, and M. Jarrell, "Cluster extension of CPA using the Dynamical Cluster Approximation," *unpublished*.

[77] M. Abolfath, T. Jungwirth, J. Brum, and A. H. MacDonald, "Theory of magnetic anisotropy in $III_{1-x}Mn_xV$ ferromagnets," *Phys. Rev. B*, vol. 63, p. 54418, 2001.

[78] T. Dietl, H. Ohno, and F. Matsukura, "Hole-mediated ferromagnetism in tetrahedrally coordinated smiconductors," *Phys. Rev. B*, vol. 63, pp. 197205/1–21, 2001.

[79] J. Piprek, *Semiconductor Optoelectronic Devices*. Academic Press, San Diego, 2003.

[80] J. Okabayashi, A. Kimura, O. Rader, T. Mizokawa, A. Fujimori, T. Hayashi, and M. Tanaka, "Core-level photoemission study of $Ga_{1-x}Mn_xAs$," *Phys. Rev. B*, vol. 58, p. R4211, 2001.

[81] M. Linnarsson, E. Janzén, B. Monemar, M. Kleverman, and A. Thilderkvist, "Electronic structure of the GaAs:Mn_{Ga}scenter," *Phys. Rev. B*, vol. 55, p. 6938, 1997.

[82] E. J. Singley, K. S. Burch, R. Kawakami, J. Stephens, D. D. Awschalom, and D. N. Basov, "Electronic structure and carrier dynamics of the ferromagnetic semiconductor $Ga_{1-x}Mn_xAs$," *Phys. Rev. B*, vol. 68, pp. 165204/1–14, 2003.

[83] H. Ohno, N. Akiba, F. Matsukura, A. Shen, K. Ohtani, and Y.Ohno, "Spontaneous splitting of ferromagnetic (Ga,Mn)As valence band observed by resonant tunneling spectroscopy," *Appl. Phys. Lett.*, vol. 73, p. 363, 1998.

[84] T. Omiya, F. Matsukura, T. Dietl, Y. Ohno, T. Sakon, M. Motokawa, and H. Ohno, "Magnetotransport properties of (Ga,Mn)As investigated at low temperature and high magnetic field," *Physica E*, vol. 7, p. 976, 2000.

[85] D. D. Betts, S. Masui, N. Vats, and G. E. Stewart, "Improved finite-lattice method for estimating the zero-temperature properties of two-dimensional lattice models," *Can. J. Phys.*, vol. 74, p. 54, 1997.

[86] A. V. Esch, L. V. Bockstal, J. D. Boeck, G. Verbanck, A. S. van Steenbergen, P. J. Wellmann, B. Grietens, R. Bogaerts, F. Herlach, and G. Borghs, "Interplay between the magnetic and transport properties in the III-V diluted magnetic semiconductor $Ga_{1-x}Mn_xAs$," *Phys. Rev. B*, vol. 56, p. 13103, 1997.

[87] S. J. Potashnik, K. C. Ku, R. Mahendiran, S. H. Chun, R. F. Wang, N. Samarth, and P. Schiffer, "Saturated ferromagnetism and magnetization deficit in optimally annealed $Ga_{1-x}Mn_xAs$ epilayers," *Phys. Rev. B*, vol. 66, p. 012408, 2002.

[88] J.-M. Tang and M. F. Flatte, "Multiband Tight-Binding Model of Local Magnetism in $Ga_{1-x}Mn_xAs$," *Phys. Rev. Lett.*, vol. 92, p. 47201, 2004.

[89] J.-M. Tang and M. F. Flatte, "Magnetic Circular Dichroism from the Impurity Band in III-V Diluted Magnetic Semiconductors," *Phys. Rev. Lett.*, vol. 101, p. 157203, 2008.

[90] J. Mašek, J. Kudrnovský, F. Máca, J. Sinova, A. H. MacDonald, and R. P. Campion, "Mn-doped Ga(As,P) and (Al,Ga)As ferromagnetic semiconductors: Electronic structure calculations," *Phys. Rev B*, vol. 75, pp. 045202/1–7, 2007.

[91] M. Turek, J. Siewert, and J. Fabian, "Magnetic circular dichroism in $Ga_{1-x}Mn_xAs$: Theoretical evidence for and against an impurity band," *Phys. Rev. B*, vol. 80, p. R161201, 2009.

[92] M. Turek, J. Siewert, and J. Fabian, "Electronic and optical properties of ferromagnetic $Ga_{1-x}Mn_xAs$ in a multiband tight-binding approach," *Phys. Rev. B*, vol. 78, p. 085211, 2008.

[93] Y. Yildirim, G. Alvarez, A. Moreo, and E. Dagotto, "Large-scale monte carlo study of a realistic lattice model for $ga1 - xmnxas$," *Phys. Rev. Lett.*, vol. 99, p. 057207, Aug 2007.

[94] D. J. Chadi and M. L. Cohen, "Tight-Binding Calculations of the Valence Bands of Diamond and Zincblende Crystals," *Phys. Stat Sol. (b)*, vol. 68, p. 405, 1975.

[95] D. J. Chadi, "Spin-Orbit Splitting in Crystalline and Compositionally Disordered Semiconductors," *Phys. Rev.*, vol. 16, pp. 790/1–7, 1977.

[96] A.-M. Nili, M. Majidi, P. Reis, J. Moreno, and M. Jarrell, "The effect of the spin-orbit interaction and attractive Coulomb potential on the magnetic properties of $Ga_{1-x}Mn_xAs$," *in preparation*, 2010.

[97] R. Kubo, "Statistical-Mechanical Theory of Irreversible Processes. I. General Theory and Simple Applications to Magnetic and Conduction Problems," *J. Phys. Soc. Jpn*, vol. 12, p. 570, 1957.

[98] A. K. Bhattacharjee and C. B. a. la Guillaume, "Model for the mn acceptor in gaas," *Sol. St. Commun.*, vol. 113, p. 17, 1999.

[99] A. Richardella, P. Roushan, S. Mack, B. Zhou, D. Huse, D. Awschalom, and A. Yazdani, "Visualising Critical Correlations Near the Metal-Insulator Transition in $Ga_{1-x}Mn_xAs$," *Science*, vol. 327, p. 665, 2010.

[100] M. Sawicki, D. Chiba, A. Korbecka, Y. Nishitani, J. Majewski, F. Matsukara, T. Dielt, and H. Ohno, "Experimental probing of intrerplay between ferromagnetism and localization in (Ga,Mn)As," *Nature Physics*, vol. 6, pp. 22/1–4, 2010.

[101] G. Acbas, M.-H. Kim, M. Cukr, V. Novak, M. A. Scarpulla, O. D. Dubon, and T. Jungwirth, "KElectronic Structure of Ferromagnetic Semiconductor $Ga_{1-x}Mn_xAs$ Probed by Subgap Magneto-optical Spectroscopy," *Phys. Rev. Lett.*, vol. 103, pp. 137201/1–4, 2009.

[102] Y. Nishitani, D. Chiba, M. Endo, M. Sawicki, F. Matsukara, T. Dietl, and H.Ohno, "Curie temperature versus hole concentration in field-effect structures of $Ga_{1-x}Mn_xAs$," *Phys. Rev. B*, vol. 81, pp. 045208/1–8, 2010.

[103] K. S. Burch, D. B. S. E. J. Singley, J. Stephens, B. L. Sheu, R. K. Kawakami, P. Schiffer, N. S. D. D. Awschalom, and D. N. Basov, "Impurity Band Conduction in a High Temperature Ferromagnetic Semiconductor," *Phys. Rev. Lett.*, vol. 97, pp. 087208/1–4, 2006.

[104] H. Morkoç, A. D. Carlo, and R. Cingolani, "GaN-based modulation doped FETs and UV detectors," *Solid-State Electronics*, vol. 46, p. 157, 2002.

[105] S. J. Pearton, F. Ren, A. P. Zhang, and K. P. Lee, "Fabrication and performance of GaN electronic devices," *Mater. Sci. Eng. R*, vol. 30, p. 55, 2000.

[106] T. P. Chow and M. Ghezzo, "SiC power devices. in III-Nitride, SiC, and Diamond Materials for Electronic Devices," in *Meterial Research Society Symposium Proceeding, Pittsburgh, PA* (D. K. Gaskill, C. D. Brandt, and R. J. Nemanich, eds.), vol. 423, pp. 69–73, 1996.

[107] M. Zajac, J. Gosk, M. Kamińska, A. Twardowski, T. Szyszko, and S. Podsiadlo, "Paramagnetism and antiferromagnetic $d-d$ coupling in GaMnN magnetic semiconductor," *Appl. Phys. Lett.*, vol. 79, p. 2432, 2002.

[108] S. Sonoda, S. Shimizu, T. Sasaki, Y. Yamamoto, and H. Hori, "Molecural beam epitaxy of wurtzite (Ga,Mn)N on sapphire (0 0 0 1) showing the ferromagnetism at room temperature," *J. Cryst. Growth*, vol. 237-239, p. 1358, 2002.

[109] S. J. Pearton, C. R. Abernathy, D. P. Norton, A. F. Hebard, Y. D. Park, L. A. Boatner, and J. D. Budai, "Advances in wide bandgap materials for semiconductor spintronics," *Mater. Sci. Eng. R*, vol. 40, p. 137, 2003.

[110] K. H. Ploog, S. Dhar, and A. Trampert, "Structural and magnetic properties of (Ga,Mn)As layers grown on SiC by reactive molecular beam epitaxy," *J. Vac. Sci Technol. B*, vol. 21, p. 1756, 2003.

[111] A.-M. Nili, U. Yu, D. Browne, J. Moreno, and M. Jarrell, "Magnetic and Transport Properties of the Diluted Magnetic Semiconductor $Ga_{1-x}Mn_xAs$ within the Dynamical Mean-Field Approximation," *in preparation*, 2010.

[112] G. Dalpian and S.-H. Wei, "Hole-Mediated Stabilization of Cubic GaN," *Phys. Rev. Lett.*, vol. 93, p. 216401, 2004.

[113] A. Kobayashi, O. F. Sankey, S. M. Volz, and J. D. Dow, "Semiempirical tight-binding band structures of wurtzite semiconductors: AlN, CdS, CdSe, ZnS, and ZnO," *Phys. Rev. B*, vol. 28, p. 935, 1983.

[114] S. Schulz, S. Schumacher, and G. Czycholl, "Tight-binding model for semiconductor quantum dots with a wurtzite crystal structure: From one-particle properties to Coulomb correlations and optical spectra," *Phys. Rev. B*, vol. 73, p. 245327, 2006.

[115] N. Furukawa, "Thermodynamics of the Double Exchange Systems," in *Physics of Manganites* (Kaplan and Mahanti, eds.), pp. 1–38, Plenum, 1999.

[116] L. Bergqvist, O. Eriksson, J. Kudrnovský, V. Drchal, P. Korzhavyi, and I. Turek, "Magnetic Percolation in Diluter Magnetic Semicondoctors," *Phys. Rev. Lett.*, vol. 93, p. 137202, 2004.

Appendix: Permissions

The author has the right to use the article or a portion of the article in a thesis or dissertation without requesting permission from APS, provided the bibliographic citation and the APS copyright credit line are given on the appropriate pages.

From the website of the American Physical Society (APS).

Vita

Abdolmadjid Nili was born in December 1975, in Tehran, Iran. He finished his undergraduate studies at Sharif University of Technology in February 1999. He earned a master of science degree in physics from University of Cincinnati in August 2006. In August 2008 he moved to Louisiana State University to continue his graduate studies in physics. He is currently a candidate for the degree of Doctor of Philosophy in physics, which will be awarded in August 2010.